DETERMINATION OF PROCESS MAP FOR HOT FORMING OF Ti-6Al-4V

A MASTER'S THESIS

in

Manufacturing Engineering

Atilim University

by

YASİN DEMİRKOL

APRIL 2018

DETERMINATION OF PROCESS MAP FOR HOT FORMING OF Ti-6Al-4V

A THESIS SUBMITTED TO

THE GRADUATE SCHOOL OF NATURAL AND APPLIED SCIENCES

OF

ATILIM UNIVERSITY

BY

YASİN DEMİRKOL

IN PARTIAL FULFILLMENT OF THE REQUIREMENTS FOR THE DEGREE OF

MASTER OF SCIENCE

IN

THE DEPARTMENT OF MANUFACTURING ENGINEERING

APRIL 2018

Approval of the Graduate School of Natural and Applied Sciences, Atilim University.

_____

Prof. Dr. Ali Kara

Director

I certify that this thesis satisfies all the requirements as a thesis for the degree of Master of Science.

_____

Prof. Dr. Engin S. Kılıç

Head of Department

This is to certify that we have read the thesis “Determination of Process Map for Hot Forming of Ti-6Al-4V” submitted by “Yasin DEMİRKOL” and that in our opinion it is fully adequate, in scope and quality, as a thesis for the degree of Master of Science.

_____

Dr. Caner Şimşir

Supervisor

Examining Committee Members

Dr. Omer Music _____

Dr. Kemal Davut _____

Dr. Caner Şimşir _____

Date: 24.04.2018

I hereby declare that all information in this document has been obtained and presented in accordance with academic rules and ethical conduct. I also declare that, as required by these rules and conduct, I have fully cited and referenced all material and results that are not original to this work.

Name, Last name: Yasin DEMİRKOL

Signature:

ABSTRACT

DETERMINATION OF PROCESS MAP FOR HOT FORMING OF Ti-6Al-4V

Demirkol, Yasin

M.S., Manufacturing Engineering Department

Supervisor: Dr. Caner Şimşir

April 2018, 64 pages

Titanium alloys are used in the field of aviation, turbine blades, gas turbines and engine parts, propellers and many other parts because of their resistance to corrosion as well as their high strength to weight ratio. However, in order to take advantage of these properties, titanium alloys having low ductility at room temperature require high temperature forming techniques which have inherent disadvantages. Hot forging is the most common method for manufacturing these components.

Titanium hot forging is more complicated than conventional steel forging due to many reasons: flow instabilities that may occur during forging, macro-micro cracks, static and dynamic strength loss due to melting at grain boundaries and heterogeneous microstructure and alpha layer formation due to air interaction are most common problems. More important than these, the microstructure formed during the titanium alloys forging cannot be repaired by the post-forging heat treatment as opposed to many steels. For this reason, titanium forging must be designed as a "thermo-mechanical-metallurgical process", not only as a forming process.

In this work, the material data required for designing the hot forging process of the Ti-6Al-4V alloy to satisfy the above conditions was obtained by experimental methods. A wide range of temperature and strain rate controlled compression tests was performed to find the material law parameters that determine the behavior of the material in the plastic region. A "Process Map" was generated which restricts the amount of temperature, deformation amount and speed to obtain forged products without any problems and desired microstructure.

Keywords: Titanium, Forging, Mechanical characterization, Flow curve, Process map

ÖZ

Ti-6Al-4V ALAŞIMININ SICAK ŞEKİLLENDİRMESİ İÇİN SÜREÇ HARİTASININ BELİRLENMESİ

Yasin,Demirkol

Yüksek Lisans, İmalat Mühendisliği Bölümü

Tez Yöneticisi: Dr. Caner Şimşir

Nisan 2018, 64 sayfa

Titanyum alaşımları, hafif ve mukavemetli olmalarının yanı sıra korozyona karşı dirençleri sebebiyle havacılık alanında, türbin bıçakları, gaz türbin ve motor parçaları, pervaneler gibi birçok parçanın imalatında kullanılmaktadır. Fakat, bu avantajlardan yararlanabilmek oda sıcaklığındaki düşük süneklikleri nedeniyle, titanyum alaşımlarının genellikle kendine özgü başka sıkıntıları olan yüksek sıcaklık hacimsel ve sac şekillendirme yöntemlerine ihtiyaç duyulmaktadır. Sıcak dövme işlemi bu bileşenlerin imalatı için en yaygın kullanılan yöntemdir.

Titanyum sıcak dövme işlemi geleneksel çeliklerin dövme işlemine göre birçok sebepten dolayı daha karmaşıktır: Dövme sırasında oluşabilen akış kararsızlıkları, makro/mikro çatlaklara sebep olması, tane sınırlarında erime ve heterojen içyapı nedeniyle statik ve dinamik mukavemet kaybı, havayla etkileşimden dolayı alfa tabakası oluşumu en sık karşılaşılan problemlerdir. Bunlardan daha önemlisi titanyum dövme sırasında oluşan içyapı birçok çeliğin aksine dövme sonrası yapılan ısıl işlemde onarılamamaktadır. Bu nedenle titanyum dövme işlemi sırf bir şekillendirme işlemi olarak değil, ürüne "özellik kazandırılan" bir termo-mekanik-metalurjik bir süreç olarak tasarlanmalıdır.

Bu çalışmada, Ti-6Al-4V alaşımının sıcak kalıp dövme işleminin yukarıdaki belirtilen şartları sağlayacak şekilde tasarımı için gerekli olan malzeme verisi, deneysel yöntemlerle elde edilmiştir. Malzemenin plastik bölgedeki davranışını belirleyen malzeme yasası parametrelerini belirlemek için geniş yelpazede sıcaklık ve genleme

hızı kontrollü basma testleri gerçekleştirilmiştir. Hatasız, istenilen içyapıda dövme ürününün elde edilmesi için deformasyon miktarı ve hızlarını kısıtlayan “Süreç Haritası” elde edilmiştir.

Anahtar kelimeler: Titanyum, Dövme, Malzeme karakterizasyonu, Akma eğrisi, Süreç haritası

ACKNOWLEDGEMENTS

I would first like to thank my thesis advisor Dr. Caner Şimşir for his guidance, comments and intense encouragement during the study. I also would like to thank to Dr. Omer Music for his valuable comments and suggestions. Without great support of Dr. Caner Şimşir, Dr. Omer Music and Dr. Kemal Davut, this study would not be possible to complete. Their knowledge is like a helping hand for my research topic and also my career.

I have performed all my studies in Metal Forming Centre of Excellence (MFCE) and I would like to thank director of MFCE Dr. Besim Baranoğlu.

A special thanks to Res. Eng. Rasim Köksal Ertan for his precious help and support which made the achievement of this thesis possible.

I would like to express my deep love to my parents and my brother; Ayten, Ali and Ali Mert Demirkol for their priceless support during the study.

Finally, I must express my very profound gratitude to my wife; Elçin Demirkol for providing me with unfailing support and continuous encouragement throughout my study and writing this thesis. This accomplishment would not have been possible without her. Thank you.

TABLE OF CONTENTS

LIST OF TABLES

LIST OF FIGURES

LIST OF ABBREVIATIONS

3D	: Three Dimensional
ASTM	: American Society for Testing and Materials
BCC	: Body Centered Cubic
DMM	: Dynamic Material Model
DR	: Dynamic Recovery
DRX	: Dynamic Recrystallization
EDM	: Electrical Discharge Machine
ELI	: Extra Low Interstitials
FEA	: Finite Element Analysis
FFT	: Fast Fourier Transform
GRG	: Generalized Reduced Gradient
HCP	: Hexagonal Close Packed
LVDT	: Linear Variable Differential Transformers
MFCE	: Metal Forming Center of Excellence
NPL	: National Physics Laboratory
PID	: Proportional–Integral–Derivative
SPF	: Superplastic Forming
TC	: Thermocouple
Ti64	: Ti-6Al-4V
VF	: Void Formation
WC	: Wedge Cracking

NOMENCLATURE

ε_t	: True strain
$\Delta\varepsilon$	: Strain increment
$\dot{\varepsilon}$	: Strain rate
σ_a	: Actual flow stress
σ_{fc}	: Corrected flow stress
σ_t	: True stress
μ	: Friction coefficient :
η	: Efficiency parameter
ζ	: Instability parameter
c	: Correction factor
d_0	: Initial diameter
d_i	: Instantaneous diameter
h_0	: Initial height
h_i	: Instantaneous height
m	: Strain rate sensitivity
$\bar{m}$	: Friction factor
A_0	: Initial area
A_i	: Instantaneous area
$A,m_1,..m_9$	: Hänsel-Spittel model material constants
B	: Barreling coefficient (NPL)
F	: Force
T	: Temperature
ΔT	: Temperature rise

INTRODUCTION

Ti-6Al-4V alloy which is used in this study is one of the most commonly used titanium alloys. It has low density and high strength, good corrosion and erosion resistance to different environment, good oxidation resistance, and moderate strength at high temperatures, making it valuable for industrial applications. The features which make this alloy different from other light metals are complex and interesting. The microstructure and the process of Ti-6Al-4V is complicated. However, its excellent properties make it the most widely used titanium alloy.

The microstructure has a great effect on the deformation and fracture behavior and on the mechanical properties of Ti-6Al-4V (will be called Ti64). It has a reversible transformation of the crystal structure from alpha (α, hexagonal close-packed) structure to beta (β, body-centered cubic) structure when the temperature reaches certain level. The complex diversity in microstructure is showed up by this allotropic behavior and it offers advantage to obtain different mechanical properties for different applications.

Ti-64 requires precisely controlled thermo-mechanical processing parameters due to its variable formability in different conditions. The hot workability of the alloy decreases strongly with reducing deformation temperature. Because of this situation it is considered to be difficult to process[1]. The processing parameters such as temperature, strain and strain rate, influence the flow behavior of Ti-64 during thermo-mechanical processing[2]. As mentioned, the initial microstructure has a strong effect on the hot working behavior. Therefore it is very important to determine the deformation behavior of the material for a specific initial microstructure.

The change of the flow behavior in the permanent deformation zone of the materials during the metal forming processes with the parameters such as the amount of deformation, temperature, deformation rate is defined by material law. Mechanical tests with various conditions of the relevant parameters are required in order to determine the material law. True stress and true strain curves obtained from the mechanical tests are used to obtain flow curves by making necessary corrections.

Determining flow curves is an essential step to obtain process map which is an effective tool that determines the behavior of the material. The process map consisting of superimposed efficiency and instability maps provides the temperature and strain rate ranges required to ensure accurate and desired product in addition to the material flow and loads provided by the flow curves.

A series of approaches and methods have been used to characterize the hot forming process. Front and Ashby[3] introduced a deformation map which shows the dominant flow mechanism areas for a given test condition. Yet only pure metals and some alloys were applied to obtain the map. Raj[4] established a damage nucleation map which shows the nucleation of deformation as a function of temperature and strain rate. Semiatin and Jonas[5] have developed flow localization parameters based on force equilibrium and it was related to the work hardening and the strain rate sensitivity parameter. Prasad and Gegel[6] have developed the so-called dynamic material model (DMM) under which the work piece is considered as a dissipater of power. The study assumed the strain rate sensitivity parameter a constant.

When studies on Ti-64 and other methods are examined; Seshacharyulu and Prasad[7] determined the influence of an equiaxed ($\alpha+\beta$) preform microstructure upon the forging response. Łukaszek-Sołek and Krawczyk[8] evaluated the activation energy for deformation and showed the relation between Zener-Hollomon parameter and flow stress. Braga and Barbosa[9] used slightly different version of the Zener-Hollomon equation to determine the behavior of Ti-64 below the beta transus. Tello and Gerlich[10] used the Sellars and Tegart equation to determine the behavior of the alloy above the beta transus. Park and Yeom[11], established a simulation tool for prediction of Ti-64 deformation behavior. Obtained processing maps were implemented into Finite Element Analysis. Lee[12], studied sensitivity of the temperature during deformation and the effects of the strain, strain rate and temperature on hot flow behavior of Ti-64. The study was also supported by microstructural examination. Calvert and Pollard[13], studied several hot flow stress model and compare them in terms of compatibility between predicted and measured flow stress. They indicated that developing an accurate flow stress model is very important and must be supported by reliable physical experiments. Opela and Schindler[14] evaluated a hot flow stress

model by the help of Hänsel-Spittel parameter to be able to implement the model in FEA software, Transvalor FORGE.

For the above consideration, this study concentrated on the following areas:

- to study the deformation behavior of Ti-64 by conducting a wide range of isothermal compression tests at six different strain rates and four different temperatures.
- to study the effect of friction by applying different barreling correction methods.
- to determine Hänsel-Spittel flow model parameters of the alloy.
- to determine the processing map by implementing dynamic material modeling method with a variable strain rate sensitivity parameter.

Structure of the thesis

This thesis is organized into four separate chapters.

Chapter 1 sets out the main purpose of the work. It also introduces the general overview of titanium and its alloys and the methods used in the study.

Chapter 2 presents the test system, specimen preparation and the procedure followed during the experiments. The experimental methods was elaborated how to obtain proper and reliable data to determine the process map.

Chapter 3 covers the experimental flow stress behavior of Ti-64 and the methods used for flow stress correction such as friction, deformation heating and load cell ringing. Obtaining the constitutive law was also explained.

Chapter 4 covers the efficiency and instability map which provide detailed deformation map of Ti-64.

CHAPTER 1

BACKGROUND & LITERATURE REVIEW

In 1791, a new material was discovered by Reverend William Gregor in the Menachan valley of Cornwall in England who named it menachite. A few years later this material was rediscovered by German chemist Martin Heinrich Klaproth. Klaproth was inspired by the Titans who represented the power of the Greek mythology and denominated the material as Titanium.

Titanium is alloyed with iron, aluminum, vanadium, molybdenum etc. elements to obtain strong and lightweight alloy. It has the highest corrosion resistance and strength-density ratio among the metallic alloys. Titanium can be used as refractory metal under favor of its relatively high melting point.

1.1. Titanium and its Alloys

There are many different applications in the field of titanium alloys. These alloys are highly preferred in petrochemical and marine areas due to their resistance to corrosion. Biocompatibility feature is used as an artificial support component in bone fracture treatment. There are also quite a few applications in consumer goods such as watches, jewelry, cameras and sports equipment. But the most used area of titanium alloys is the aviation industry. It is used extensively in compressor discs, airframe structure, turbine blades, space rockets and satellites as it provides light and economic conditions, which is the most important requirement in aviation. Figure 1 shows the comparison of specific strength and temperature for different metals.

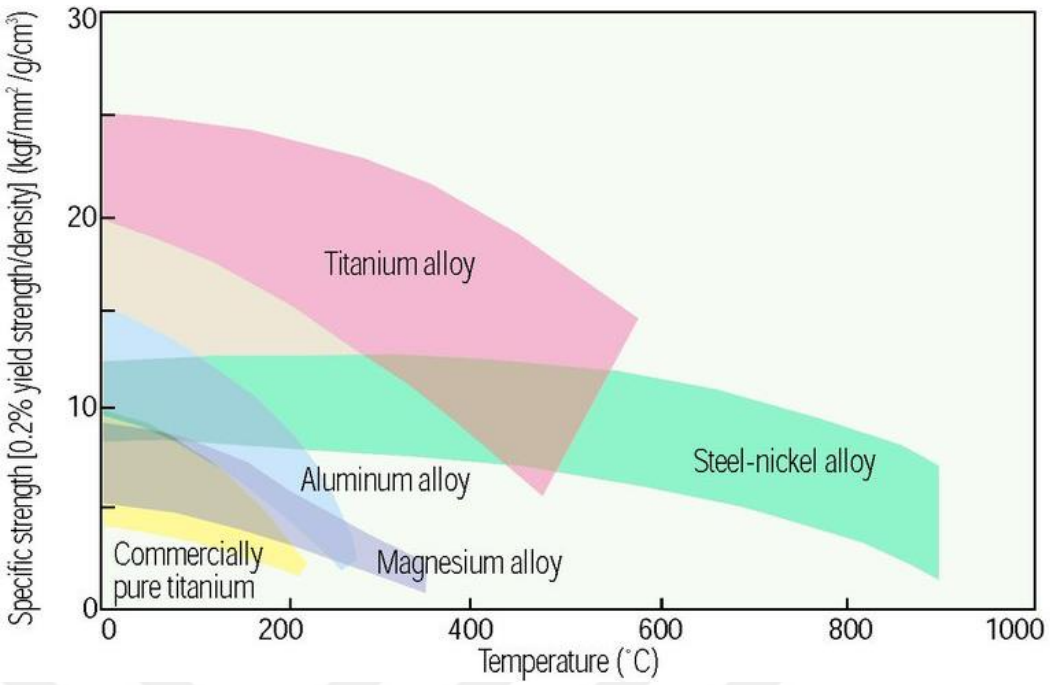

Figure 1- Comparison of specific strength and temperature for different metals[15]

As can be seen, titanium alloys have a higher specific strength than other metals up to 400-500°C.

Pure titanium has an allotropic transformation when the temperature is raised through 882°C from hcp (α) to bcc (β) as it can be seen in Figure 2.

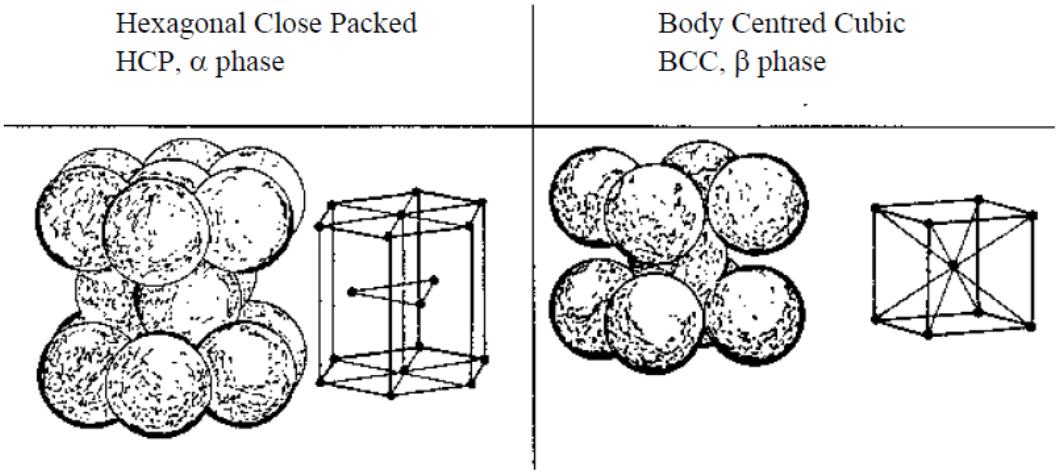

Figure 2- HCP and BCC structure[16]

Alloying elements dissolved in the titanium can either stabilize α phase by rising the α+β transition temperature or stabilize β phase by lowering the α+β transition temperature or act only as solid solution strengtheners and not influence the transition temperature. Interstitial elements such as nitrogen, carbon and especially oxygen are strong α phase stabilizers while hydrogen is β stabilizer. The increase in the amount of interstitial elements causes a severe increase in strength, while at the same time it causes the ductility to decrease drastically. Table 1 shows alloying element and their stabilizing effect.

Alloying element	Range (wt%)	Effect on structure
Aluminium	2 to 7	Alpha stabilizer
Tin	2 to 6	Alpha stabilizer
Vanadium	2 to 20	Beta stabilizer
Molybdenum	2 to 20	Beta stabilizer
Chromium	2 to 12	Beta stabilizer
(Copper)	2 to 6	Beta stabilizer
Zirconium	2 to 8	Alpha and beta strengthening
Silicon	0.2 to 1	Improves creep resistance

Table 1- Alloying elements and their stabilizing effects[16]

Titanium alloys are divided into three main groups according to the amount and the type of alloying elements.

Since pure titanium and titanium alloy with α stabilizers aluminum and tin are hcp at ordinary temperatures, they are classified as α alloy. The outstanding properties of these alloys are strength, toughness, creep resistance and weldability. The absence of ductile-to-brittle fracture behavior, the property of bcc alloys, makes alpha alloys favorable for cryogenic applications.

α+β alloys contain one or more alpha and beta stabilizers. The amount of beta stabilizers in these alloys is larger (4 to 6%)[17]. Beta alloys can be heat treated to obtain various microstructures and mechanical properties. So that mechanical properties covering a wide range can be obtained. Alpha-beta alloys exhibit good manufacturability, high strength at room temperature and acceptable strength at high temperatures.

Alloys with more than 30wt% percent β stabilizers are β alloys[17]. The beta alloys, which are in fact metastable, become partially alpha phase when elevated to relatively high temperatures. Beta alloys have good toughness, ductility and very good formability besides their low strength. Figure 3 shows a schematic relationship between the influences of alloying elements on structure.

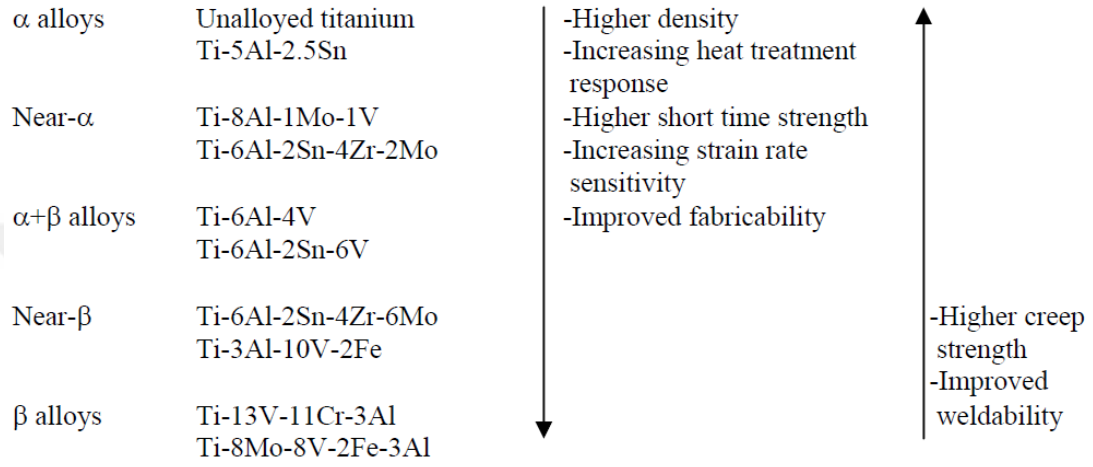

Figure 3- Relationship between alloys and their mechanical properties[16]

Alpha-beta alloy Ti-64 is an alloy containing alpha stabilizer aluminum with 6wt% and beta stabilizer vanadium with 4wt%. At room temperature and equilibrium conditions, it contains mainly alpha phase and some retained beta phase. There are many types of microstructure depending on the cooling speed and heat treatment such as grain boundary allotriomorph α, globular or primary α, Widmanstätten, basket weave and martensitic.

1.2. Overview of Hot Forming of Titanium

Hot and cold forming of the titanium alloys involves forging, rolling, extrusion, drawing, spinning, and other such operations. Operations such as forging and rolling can be referred to as primary forming operations in which the basic ingot is converted into standard billets, plates, sheets, bars and wires. Secondary operations involve bending, extrusion, drawing and spinning.

Equipment used for steels has been found suitable for titanium alloys. However, forming techniques used in forming steels require a modification to deform titanium alloys. Time, temperature and pressure are the most considerable parameters while doing modifications.

The phases contained in the titanium alloys greatly influence the mechanical properties and formability according to their amount, size and morphology. In general, the higher content of beta stabilizers increases the forgeability. However the excessive amount of beta stabilizers cause the beta transus temperature to decrease, thereby increasing the yield stresses in the alpha-beta alloy forging and consequently forging loads. Therefore, the alloy type and forging method should be decided according to the desired applications and properties.

Figure 4 presents the stress-strain graphs obtained from the hot compression test of a commonly used steel and a titanium alloy. While steels usually exhibit work hardening behavior, titanium alloys exhibit work softening behavior especially at high strain rate deformations. The behavior of work softening causes inhomogeneous strain distributions in forged parts as strain increase. Moreover, the low thermal conductivity of titanium causes temperature inhomogeneity in addition to the strain inhomogeneity that occurs during deformation.

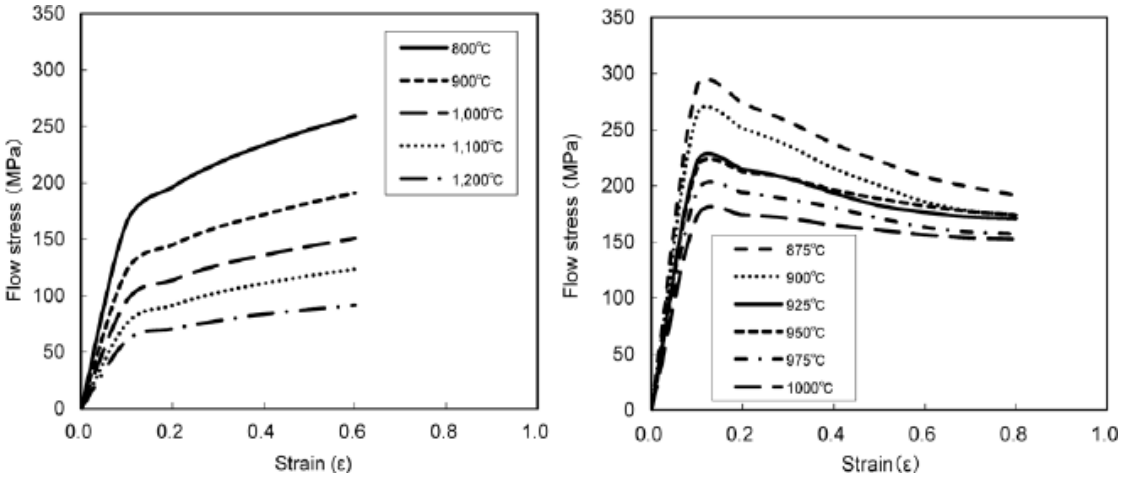

Figure 4- Schematic illustration of flow curves of steel (left) and titanium (right)[18]

CHAPTER 2

EXPERIMENTALS METHODS

2.1. Mechanical Characterization

Mechanical characterization is the fundamental and general process of measurement, in which the properties of a material are investigated and measured. During the metal forming process, the flow behavior of the materials in the permanent deformation zone is described by the material law with the parameters such as the amount of deformation, temperature, deformation rate. In order to determine the material law in hot metal forming processes, mechanical tests (tensile, compression, torsion etc.) are usually carried out with systematic variation of the relevant parameters. The true stress-true permanent strain curves obtained from the tests performed under different conditions are processed to obtain the flow curves.

For the analysis of the deformation in the material, the stress state should be determined. It is possible to calculate stresses acting at three points perpendicular to each other passing through a point and finding the stress state at that point. As the angle of a plane increases, the normal stress in that plane increases and the shear stress in the same plane decreases to zero. This plane of the maximum normal stress and the zero shear stress is called the principal plane and the normal stress acting on this plane is called the principal stress. The strains that are related to these stresses are principal strains. The diagram showing the orientation of the planes is given in Figure 5.

The stress system, which controls the flow behavior of the material, can be presented with three principal stresses, σ_1, σ_2, σ_3. In the axial compression test, ε_1 and ε_2 are the strains perpendicular to the length and equal to -1/2 of the length strain ε_3 in the ideal test, where there is no barreling.

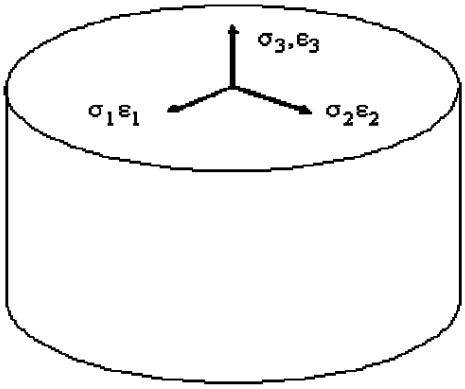

Figure 5- Illustration of stress and strain axes in compression test specimen[19]

2.2. Material

The billets 130 mm in diameter and 300 mm in height were supplied from Enpar, Germany. The round bars were hot formed and machined. An annealing of 750°C – 120 minute heat process was applied to billets. The composition of the material is shown in Table 2.

Al	V	Fe	C	N	H	O	Ti
6.18	4.08	0.14	0.014	0.004	0.0006	0.134	Balance

Table 2- Composition of the Ti-64

It was reported that the microstructure of the alloy was composed of the nearly equiaxed primary alpha (55%) and transformed beta (45%) components.

In order to confirm the results of report, microstructure analysis was carried out in the metallography laboratory of MFCE and presented in Figure 6. The structure is bi-modal containing α and β. Areas that appear light and dark color are primary-α and β domains, respectively. At 500x magnification, it appears that the dark regions are acicular-α with fine structure. The general properties of the structure are determined by the area ratio of the primary-α and the transformed β regions as well as the average sizes. Table 3 and 4 presents the phase fraction and average grain sizes of Ti64, respectively.

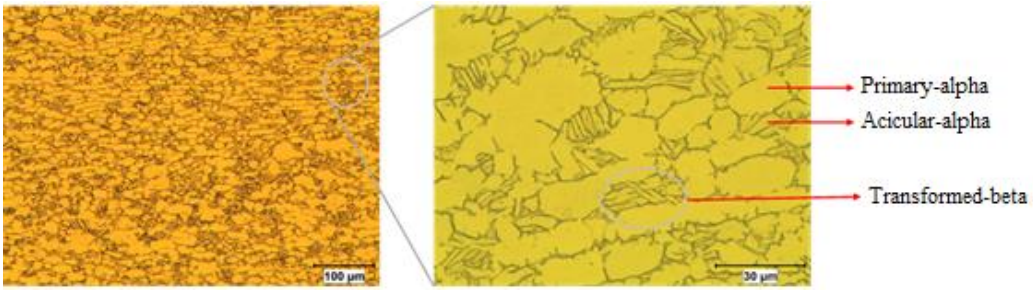

Figure 6- The initial microstructure of the Ti64 specimen obtained by optical microscopy at 100x (left) and 500x (right) magnification before the compression test

	Volumetric Phase Fraction of Transformed-beta	**Volumetric Phase Fraction of Inter-acicular-beta**
Mean Value (%)	45.5	6.9
Standard Deviation	0.4	0.60
%95 Confidence Interval	0.5	0.43
Relative Accuracy	% 1.13	% 6.94
Volume Fraction	**45.5 ± 0.5**	**6.9 ± 0.43**

Table 3- Phase fraction of Ti64

	Primary Alpha	**Transformed Beta**
Average of Horizontal Intersection	16.4	6.8
Average of Vertical Intersection	11.9	5.6
Mean Value (μm)	13.7	6.1
Standard Deviation	0.50	0.97
%95 Confidence Interval	1.2	0.6
Relative Accuracy	% 8.8	% 10.1
Average Grain Size(μm)	**13.7 ± 1.2**	**6.1 ± 0.6**
Average Grain Size(ASTM – G no)	**9.4 ± 0.2**	**11.8 ± 0.2**

Table 4- Average grain size of Primary Alpha and Transformed Beta

2.3. Hot Compression Test

During the compression testing; displacement from the LVDT (Linear Variable Differential Transformers) and applied force from the load cell are monitored and recorded. Figure 7 shows the specimen placed between the platens and the compression test setup. A uniaxial cylinder with initial height h_o is deformed to an instantaneous height of h_i resulting in the expansion of the initial diameter d_o following the law of volume conservation:

$$A_0 = A_i \tag{1}$$

$$d_0 * h_0 = d_i * h_i \tag{2}$$

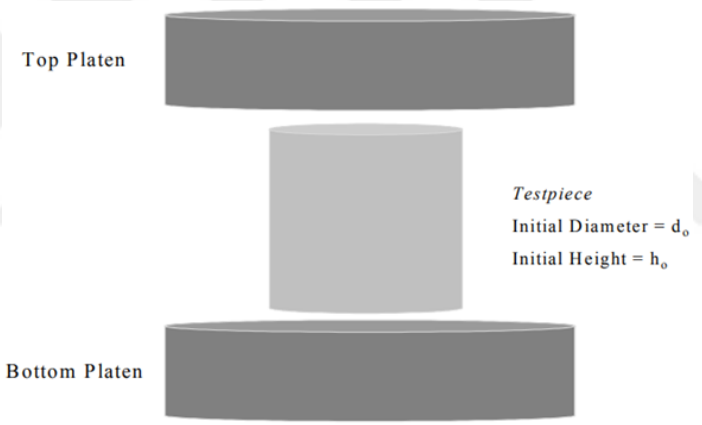

Figure 7- Diagram of an axisymmetric compression test

The definition of the true stress is dividing the load by the instantaneous cross-sectional area A_i of the cylinder with diameter d:

$$\sigma_t = \frac{F}{A_i} \tag{3}$$

True strain can be described as instantaneous in height with respect to the initial height:

$$\varepsilon_t = \ln\left(\frac{h_i}{h_0}\right) \tag{4}$$

The logarithmic strain is obtained by integrating this incremental strain:

$$\varepsilon_t = \int_{h_0}^{h_i} \frac{dh}{h_i} \tag{5}$$

Strain rate is the change in strain or deformation of a material with respect to time. Strain rate can be calculated as in Equation 6.

$$\dot{\varepsilon} = \left(\frac{1}{h_i}\right) * \frac{dh}{dt} = \frac{v(t)}{h_i} \tag{6}$$

h_i is the instantaneous height of the specimen where v(t) is the stroke speed of the system. Compression tests can be performed either with constant stroke rate or constant strain rate. Experiments with conventional machines are mostly carried out with constant strain rate.

In order to analyze the stress-strain curves properly, it is necessary to carry out tests with constant strain rate control. As can be seen in Figure 8, in the compression test for 15 mm/sec constant stroke rate with a cylindrical specimen height of 15 mm, the strain rate decreases exponentially as the strain amount increases. This behavior increases the amount of stress in the material.

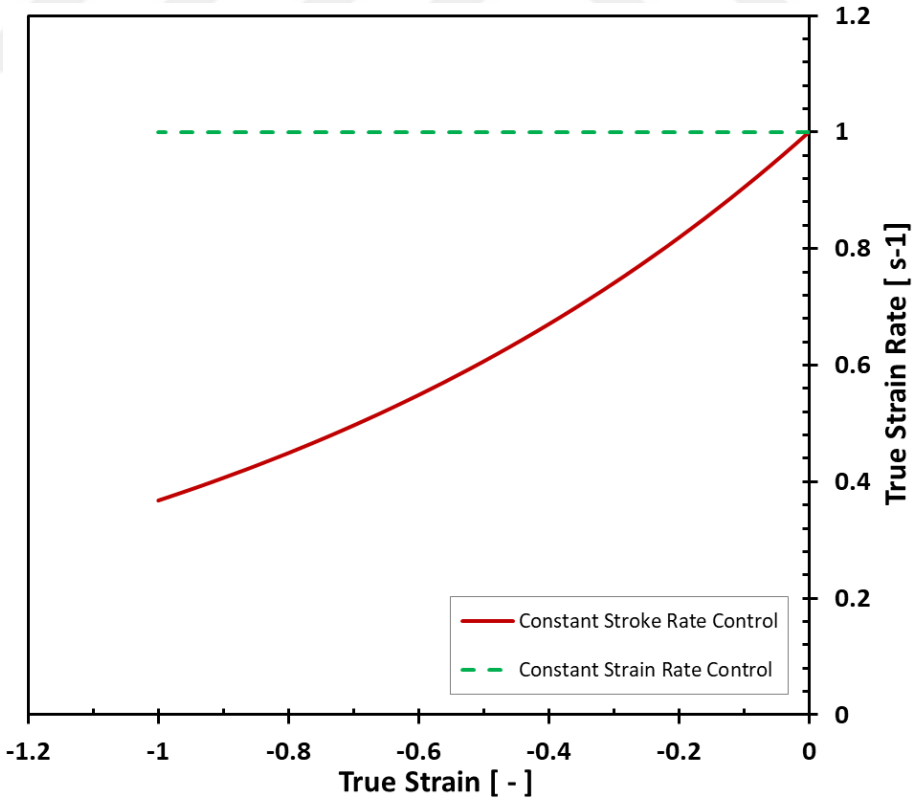

Figure 8- Comparison of stroke and strain rate control

The stroke speed must be decreased exponentially as strain increases to achieve constant strain rate in compression tests. Owing to this feature of the Gleeble system, experiments were carried out at constant true strain rate.

Test system can give true stress and true strain values. These values compared with manually calculated true stress and true strain values and there were absolutely same. After checking this, flow stress calculation made by automatically calculated values obtained from the system.

2.3.1 Test System

Hot uniaxial compression tests were carried out on the Hydrawedge® II unit of the Gleeble® 3800 Thermo-Mechanical Simulator, designed and manufactured by Dynamic Systems Inc.. The system is a Thermo-Mechanical Simulation machine with a closed-circuit thermal and mechanical control system. The heating is performed by direct current method. On the strength of jaws with high thermal conductivity and advance quench systems, cooling rate can reach up to 10000° C/s. Owing to the direct resistance heating method and the closed-loop thermal control, the temperature homogeneity is much higher than conventional furnaces.

The system with servo-hydraulic is capable of exerting 20 tons. With strokes capable of running at a minimum speed of 0.001 mm/s, a maximum speed of 2000 mm/s and a closed-loop mechanical control unit, it can achieve 10^{-3} s^{-1} to 10^{2} s^{-1} true strain rates encountered in conventional forging process maps.

The test chamber of the system is also a vacuum chamber. Thus the tests can be carried out under vacuum of 10^{-5} mbar. Also the test chamber can be filled with inert gases (nitrogen, argon, helium, etc.) to provide controlled atmospheric conditions. Owing to these properties, oxidation-like reactions that may occur on the surface of the sample can be prevented[20].

When all this is taken into account, Gleeble System meets all the requirements of the ASTM E209 standard[21]. Figure 9 show the test chamber of the Gleeble System.

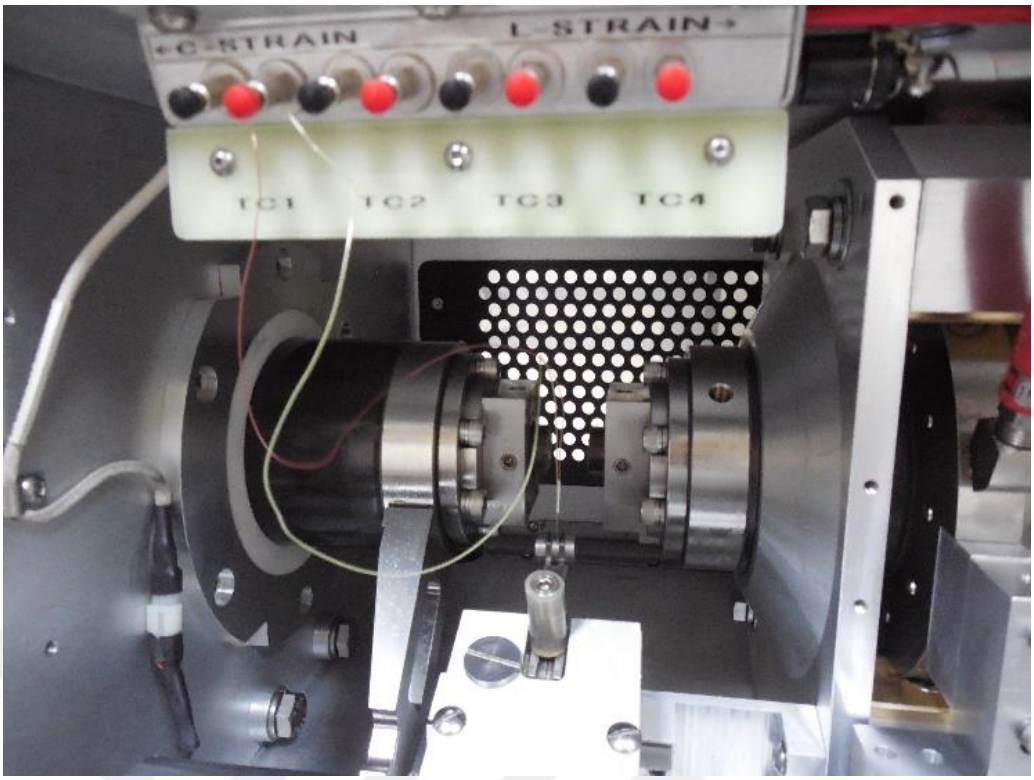

Figure 9- Test chamber of the System

2.3.2 Specimen Preparation

It has been decided to study specimens 15 mm high and 10 mm in diameter (H / D = 1.5) in the direction of ASTM E209[21]. A preliminary study has been carried out in order to ensure conformity to either the sample technical drawing or the dimensional tolerances and surface roughness values recommended in the literature. The sample sizes and manufacturing method are determined taking into account the sources in this area as well as the maximum load capacity of the device and the parameters (heating performance, temperature homogeneity, friction coefficient, etc.) that will provide the optimum test environment.

The billets 130 mm in diameter and 300 mm in height obtained from supplier, were sliced into 15.3 mm in the wire erosion (EDM) workshop in the MFCE and grinded to 10.1 mm in size. Compression specimens were removed from these slices. The specimen diameters were reduced to 10 mm by performing a peripheral grinding operation to reduce the high roughness on the surfaces of the specimens produced in the EDM bench and to improve the roundness. Figure 10 shows the course of the specimen preparation.

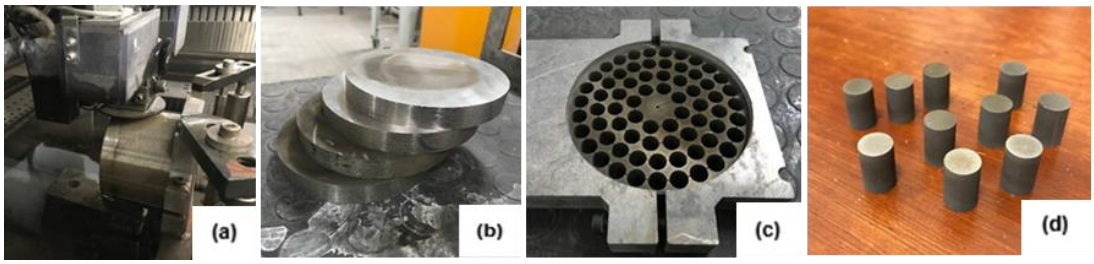

Figure 10- a) Slicing of billet in EDM **b)** Grinding of sliced billets **c)** Removing specimens from sliced billet **d)** Specimens after peripheral grinding

2.3.3 Dimensional Control

Dimensional measurements were carried out by randomly selecting 10 samples from 70 samples which were removed from each slice to confirm compliance with dimensional tolerances. Dimensional measurements were performed using the procedure recommended by the National Physics Laboratory (NPL)[22]. Figure 11 shows the height and diameter measurement points. Diameter and height measurements were performed using a micrometer with a precision of 0.0005 mm and a digital height comparator with a precision of 0.01 mm. The measurement results are presented in Tables 4. All results indicate that the necessary tolerances have been achieved. While the samples are dimensionally controlled by partial sampling (10/70) during the manufacturing, all samples were measured by the same method before each test and were not used if any sample which is out of tolerance were detected.

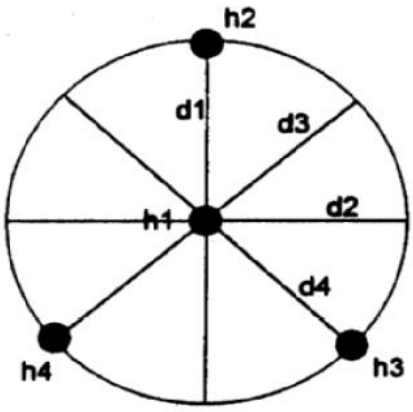

Figure 11- Height and diameter measurement points on the specimen[22]

	Diameter [mm]						Height [mm]					
Specimen	**d1**	**d2**	**d3**	**d4**	**Average**	**St. Deviation**	**h1**	**h2**	**h3**	**h4**	**Average**	**St. Deviation**
1	9.999	10.001	10	10	**10**	**0.0007**	15.011	15.014	15.014	15.01	**15.012**	**0.0018**
2	10.002	10.003	10.004	10.004	**10.003**	**0.0008**	15.029	15.03	15.022	15.026	**15.027**	**0.0032**
3	10.002	10	10.002	10.003	**10.002**	**0.0011**	15.03	15.034	15.028	15.021	**15.028**	**0.0046**
4	10.004	10	10.001	10.003	**10.002**	**0.0016**	15.027	15.02	15.033	15.041	**15.03**	**0.0075**
5	9.999	10	10	10.001	**10**	**0.0007**	15.011	15.009	15.01	15.002	**15.008**	**0.0037**
6	10.001	10.002	10	9.999	**10.001**	**0.0011**	15.009	15.008	15.007	15.007	**15.008**	**0.0006**
7	10.005	10.004	10.005	10.006	**10.005**	**0.0007**	15.012	15.005	15.001	15.006	**15.006**	**0.0037**
8	10.002	10.002	10.001	10.002	**10.002**	**0.0004**	15.02	15.019	15.025	15.024	**15.022**	**0.0027**
9	10.006	10.004	10.007	10.005	**10.006**	**0.0011**	15.027	15.027	15.027	15.028	**15.027**	**0.0004**
10	9.999	9.998	9.999	9.997	**9.9983**	**0.0008**	15.012	15.013	15.009	15.015	**15.012**	**0.0022**

Table 5- Summary of measurement results

2.3.4 Test Procedure

Tests were performed at temperatures of 850, 900, 950 and 1000°C which cover a major part of hot forming for Ti64. The target temperature was reached at a rate of 5°C/s and the sample was allowed to soak at the target temperature for 5 minutes to maintain temperature homogeneity and stabilize the microstructure. The samples were compressed to 0.4 true strain at a true strain rate of 0.001, 0.01, 0.1, 1, 10 and 100 s^{-1}. Before the long test period, Gleeble System and all its sensors (extensometers, load cells, thermocouple (TC) channels etc.) were calibrated by the manufacturer's service engineer. However, in order to establish the most appropriate experimental setup, the requirements under actual test conditions have been checked and improved.

The most important parameters affecting the yield curve and the process map determination test results are as follows: Temperature, Friction.

2.3.4.1 Temperature Control

The reliability of the results of the compression tests depends not only on the manufacturing of the specimen but also on the heating of the specimen at the desired heating rate and keeping the test temperature constant and homogeneous throughout the specimen. For this reason, prior to the temperature homogeneity test, the calibration of the TC channels done in the last technical maintenance of the relevant machine was checked and no significant deviations were found in the obtained values.

There is an acceptable deviation of only 1°C above 1000°C in each of the 3 TC channels shown in Table 6.

Calibration Value [°C]	**0**	**100**	**200**	**300**	**400**	**500**	**600**	**700**	**800**	**900**	**1000**	**1100**	**1200**	**1300**
TC1	0	100	200	300	400	500	600	700	800	900	1000	1100	1200	1300
TC3	0	100	200	300	400	500	599	699	799	899	999	1099	1199	1299
TC4	0	100	200	300	400	500	600	700	800	900	1000	1100	1200	1300

Table 6- Results of the TC calibration control

Once it has been determined that the TC channels have read the correct values, it has been checked whether the desired temperature value can be reached homogeneously on the sample. For this, the temperature distribution on the sample was measured by welding three TC's to the exact middle point of the sample, 1 mm from the left end and 1 mm from the right end.

Since the compression jaws in the Gleeble® Hydrawedge system may encounter different thermal conductivities in different materials, specimen geometries and surface roughness, the resistances have to be adjusted iteratively in real conditions to achieve efficient temperature control and homogeneous temperature distribution. Figure 12 shows the position of the resistors located behind the jaw.

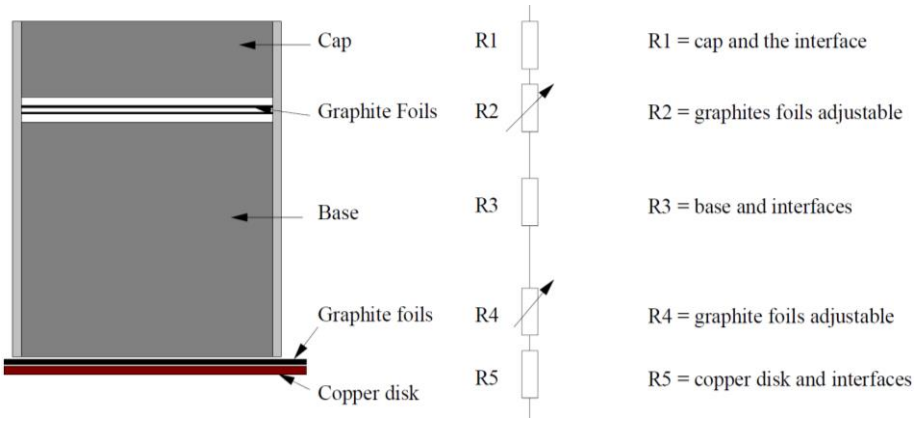

Figure 12- Resistance adjustment of Gleeble anvils[20]

By changing the number of graphite plates shown as R2 and R4 separately for each material, better temperature control is provided than the conditions required by ASTM E209. In the resistance adjustment process, 3 pieces of K-type TC's were applied to the center and ends of the specimen. The specimen was heated to 1050°C with a heating rate of 5°C/s and waited for 5 minutes at this temperature. Figure 13 summarizes the result of this study.

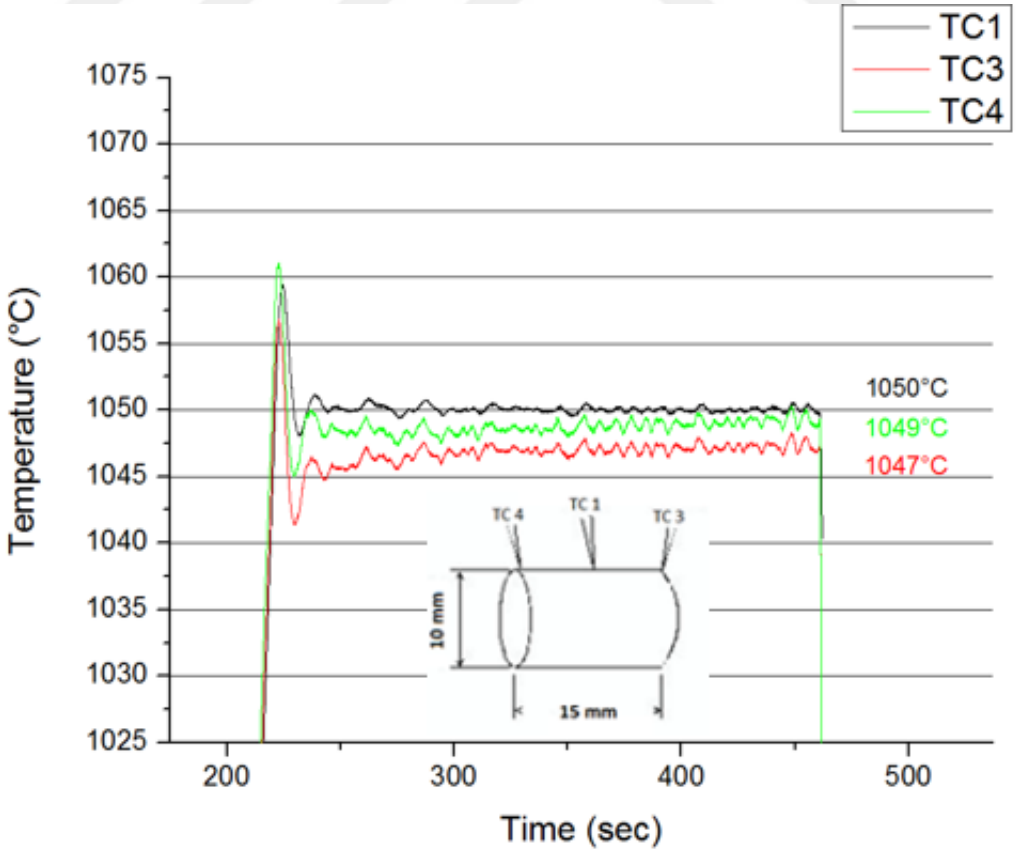

Figure 13- Temperature history of TCs after adjustments

In the first step, graphite foil thickness and number were changed to achieve temperature homogeneity of less than 5.5°C specified by the standard[21] and maximum ± 3°C difference achieved successfully. After this step, the target overshoot value was then improved by PID controls and reached below the 2% specified by the standard.

2.3.4.2 Friction Control

The friction coefficient between the specimen and the anvils must be minimized to ensure that the data obtained after the compression test is reliable. The excess coefficient of friction in the indicated region leads to an inhomogeneous deformation, shown in Figure 14, which is called barreling.

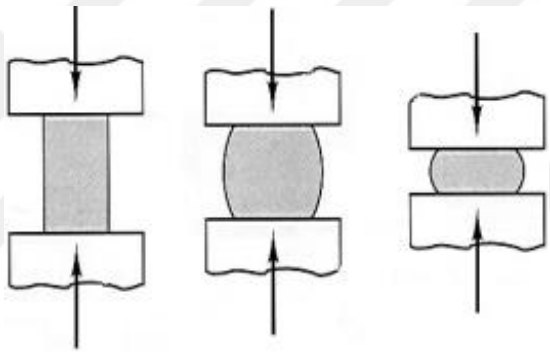

Figure 14- Barreling evolution during the test[20]

The Barreling Coefficient (B), which is defined in Equation 7, is used to quantify the amount of barreling in the compression tests.

$$B = \frac{h(d)^2}{h_0(d_0)^2} \tag{7}$$

In the equation, h_o and h denote the initial and final specimen height respectively; d_o and d denote the initial and maximum final diameter of the specimen. While the ideal value of B is 1, it is desirable to have B between 1.0-1.1 and as low as possible after compression tests[22]. Excessive barreling may cause deformation inhomogeneity and secondary tensile stress at the bulging surface which can lead to surface cracking. Figure 15 shows the effect of friction which cause bulging at the surface and cause miscalculation of workability.

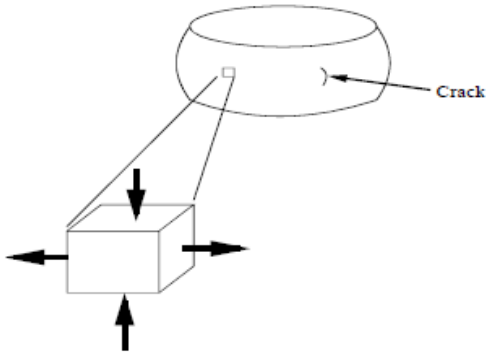

Figure 15- Secondary tensile stress generation during compression test[20]

Graphite foils and nickel paste were used between the specimen and anvils to reduce the friction coefficient in compression tests. Applying the same amount of nickel paste to both anvils is necessary for homogenous deformation.

In order to determine the acceptability of the barreling coefficient, three repetitions tests were carried out at 850°C with a strain rate of 0.1 s^{-1} up to 0.6 true strain. Height and diameter measurements were performed before and after the test as specified in Table 7, and the barreling coefficient of the specimen were determined.

	[mm]								
t1	**d1**	**d2**	**d3**	**d4**	**d5**	**d6**	**d7**	**d8**	**B**
	9.999	10.002	9.998	10.001	*14.02*	*14.035*	*14.003*	*14.007*	
	h1	**h2**	**h3**	**h4**	**h5**	**h6**	**h7**	**h8**	**1.112**
	15.0085	15.008	15.005	15.0095	*8.4975*	*8.677*	*8.449*	*8.342*	

	[mm]								
t2	**d1**	**d2**	**d3**	**d4**	**d5**	**d6**	**d7**	**d8**	**B**
	10.002	10	10.003	10.002	*14.181*	*14.085*	*14.192*	*14.179*	
	h1	**h2**	**h3**	**h4**	**h5**	**h6**	**h7**	**h8**	**1.122**
	15.012	15.013	15.0085	15.0145	*8.375*	*8.357*	*8.407*	*8.4735*	

	[mm]								
t3	**d1**	**d2**	**d3**	**d4**	**d5**	**d6**	**d7**	**d8**	**B**
	10.001	10.002	10	9.999	*14.047*	*14.063*	*14.045*	*14.06*	
	h1	**h2**	**h3**	**h4**	**h5**	**h6**	**h7**	**h8**	**1.117**
	15.03	15.0335	15.0275	15.021	*8.3435*	*8.364*	*8.592*	*8.711*	

Table 7- Specimen dimensions and barreling coefficients

d1,..,d4 and h1,..,h4 present the initial diameter and height and d5,..,d8 and h5,..,h8 present the final diameter and height, respectively. As a result of the tests it was determined that the barreling coefficient was close to the permissible value of B=1.10. In addition, repeatability of the barreling behavior was shown in experiments.

CHAPTER 3

DETERMINATION OF FLOW CURVES AND CONSTITUTIVE LAWS

3.1 Determination of Flow Curves

From the load-displacement data obtained from the test machine to the flow curves, from the flow curve to the material law parameters and to the process map, requires a large amount of digital data processing.

The data set was obtained by random selection among the 3 repeated tests for each condition. The data processing start with the sum of the load and displacement data from the machine and continue to obtain raw stress-strain graphs.

As mentioned earlier, this data is not a "flow curve" and a series correction of the stress values is required, as well as the strain. The data processing procedures applied to obtain the yield curve are summarized in Table 8.

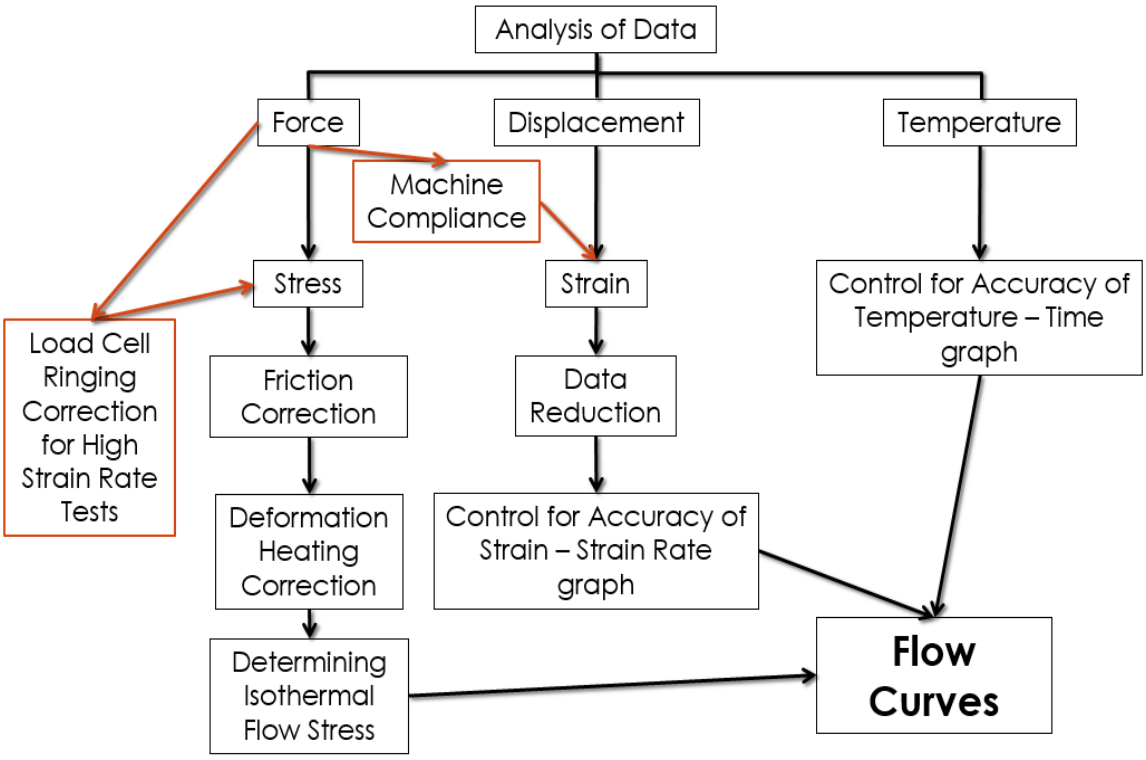

Table 8- Outline of data processing procedure

After the tests, the Strain-Temperature and Strain-Strain Rate curves were plotted and checked for any significant deviations from the test conditions.

The time required to achieve desired strain rate is very short and the system succeeded in keeping the strain rate at maximum 11% error which is far below determined by the ASTM E209 standard[21]. After it was seen that there is no significant deviation, first the strain then the stress data was corrected. A sample Strain-Temperature and Strain-Strain Rate graphs with maximum and minimum error indicators shown in Figure 16-17 respectively.

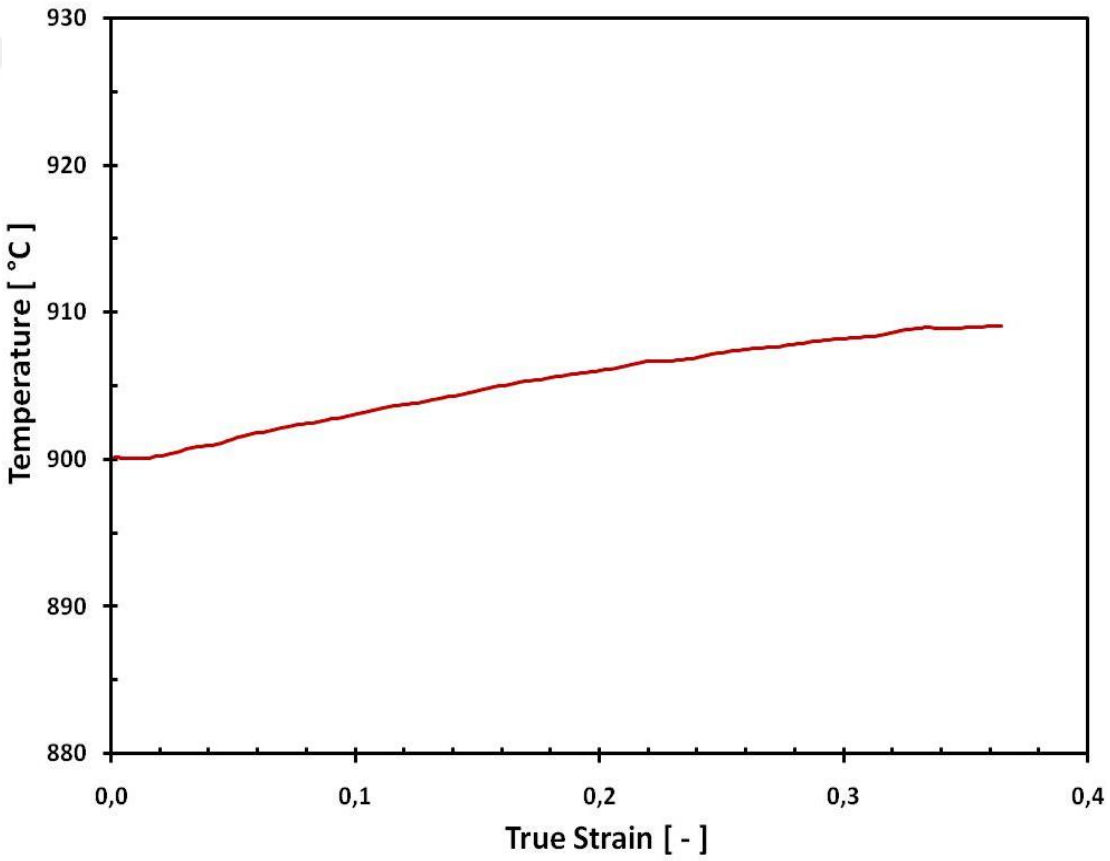

Figure 16- True Strain vs. Temperature

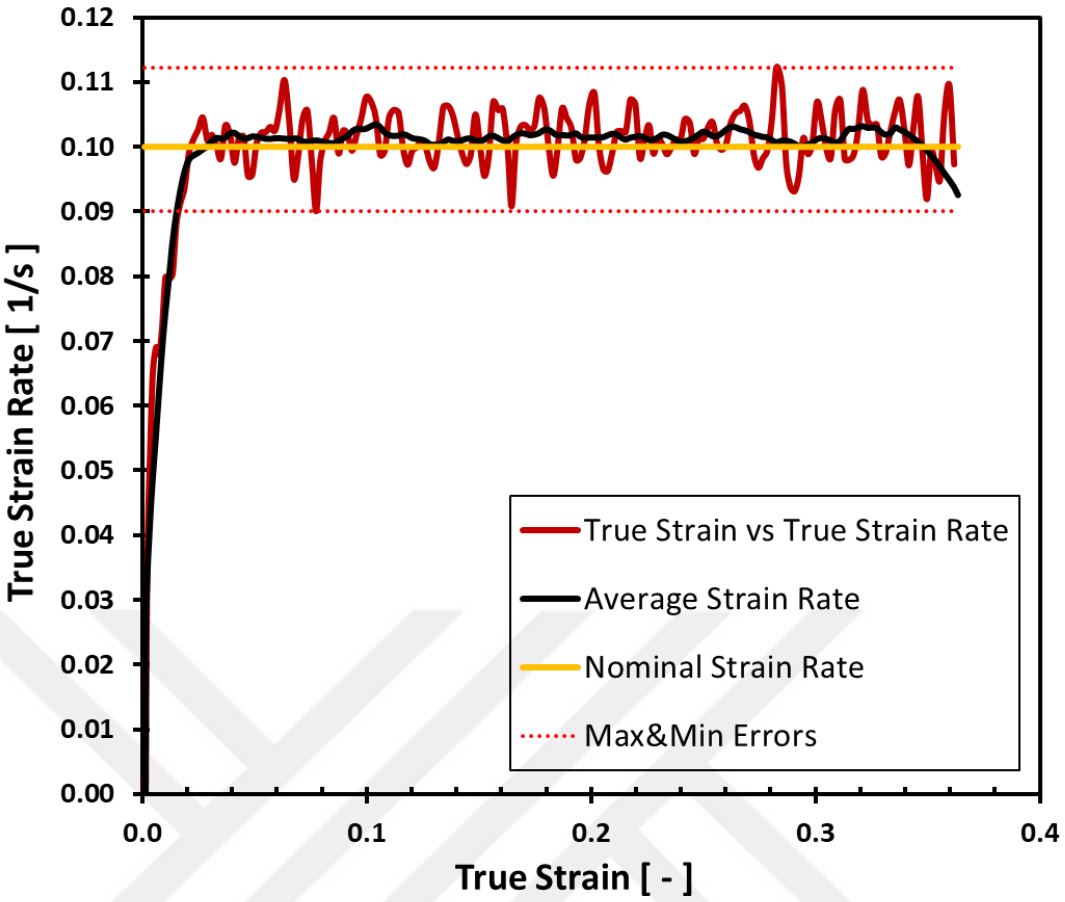

Figure 17- True Strain vs. True Strain Rate

3.1.1 Data Processing

The data acquisition rate of the test system was determined to collect data at 0.001 strain steps during the experiments. By this way, 250 data points per experiment were obtained. This amount was considered excessive for most of the analysis. The data is also not exactly synchronized due to small differences in the system. For this reason, the data is reduced and synchronized at $\Delta\varepsilon$=0.02 strain increment. The "Vlookup" function of MS Excel software is used for this process. An exemplary result is presented in Figure 18.

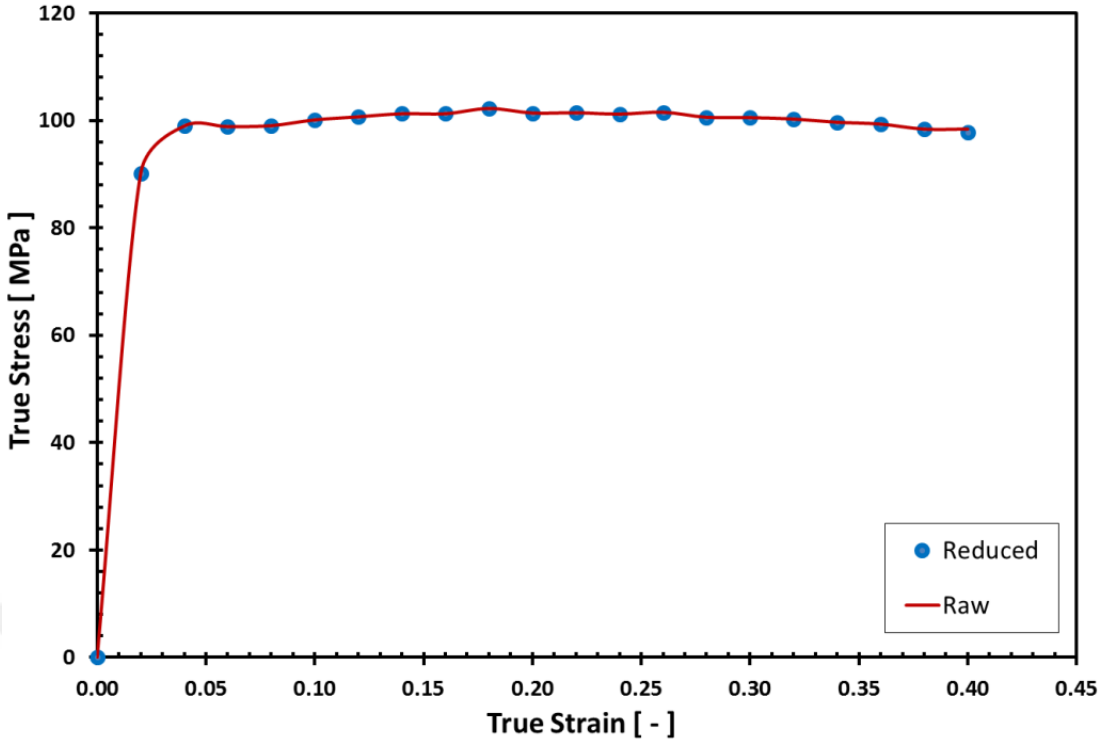

Figure 18- Comparison of the Raw and Reduced data

3.1.2 Machine Compliance

The Gleeble Hydrawedge system uses a LVDT sensor placed between the jaws to measure specimen length[20]. Thus, elastic deformation of the system do not enter into strain calculations. Since the position of the LVDT sensors is slightly behind the jaws, a small amount of jaw compliance can affect the results. The amount of machine compliance of the jaws was determined by studies on specimens with known elastic properties. Subsequent studies have shown that machine compliance correction is only necessary to determine elastic properties.

3.1.3 Friction Correction

In metal forming, friction plays an important role while stating the life of the tool, the formability of the work material and the quality of the finished product.

The effects of overheating, abrasion, etc., caused by friction, cause temperature differences on the sample, which is the result of barreling and deformation heating. The widening diameter due to the barrel causes the miscalculation of the stress.

Therefore, friction correction on the raw data is required. For this, measurements were made before and after the test as NPL suggested, and the barreling coefficients were determined.

Two different correction procedures, which are the article of Ebrahimi[23] and Evans[24], have been examined and compared on the data.

Ebrahimi's approach states that a simple method which does not need force measurement can be used to correct flow curves. In this study by means of the upper-bound theory, the constant friction factor was determined. The study stated that constant friction can be calculated only by measuring the barreling coefficient of the specimen. The constant friction factor ($\bar{m}$) can be obtained as in Equation 8;

$$\bar{m} = \frac{\frac{R}{H}b}{\frac{4}{\sqrt{3}} - \frac{2b}{3\sqrt{3}}} \tag{8}$$

Where

$$b = 4\frac{\Delta R}{R}\frac{H}{\Delta H} \tag{9}$$

And

$$R = R_0\sqrt{\frac{H_0}{H}} \tag{10}$$

In the equations, R and H denote average radius and height of the specimen after compression, respectively; ΔR and ΔH denote difference between max&min radius and reduction in height. The terms R_0 and H_0 are initial radius and height of the specimen where b is the barrel parameter.

Even if Ebrahimi's approach is easily implementable on the data, the friction condition has a strong relation and varies with strain rate and temperature.

In Evan's approach, the parameters of temperature and strain rate, which affects the friction, were examined and friction calibration curves were obtained for the coefficient of friction by the help of finite element analysis.

The coefficient of friction (μ) can be determined by using the relation of the friction constant (c) with the coefficient of barreling (B).

$$\mu = c(1 + B^{1/2}) \tag{11}$$

By taking advantage of Figure 19, new friction coefficients are calculated by using barreling coefficient.

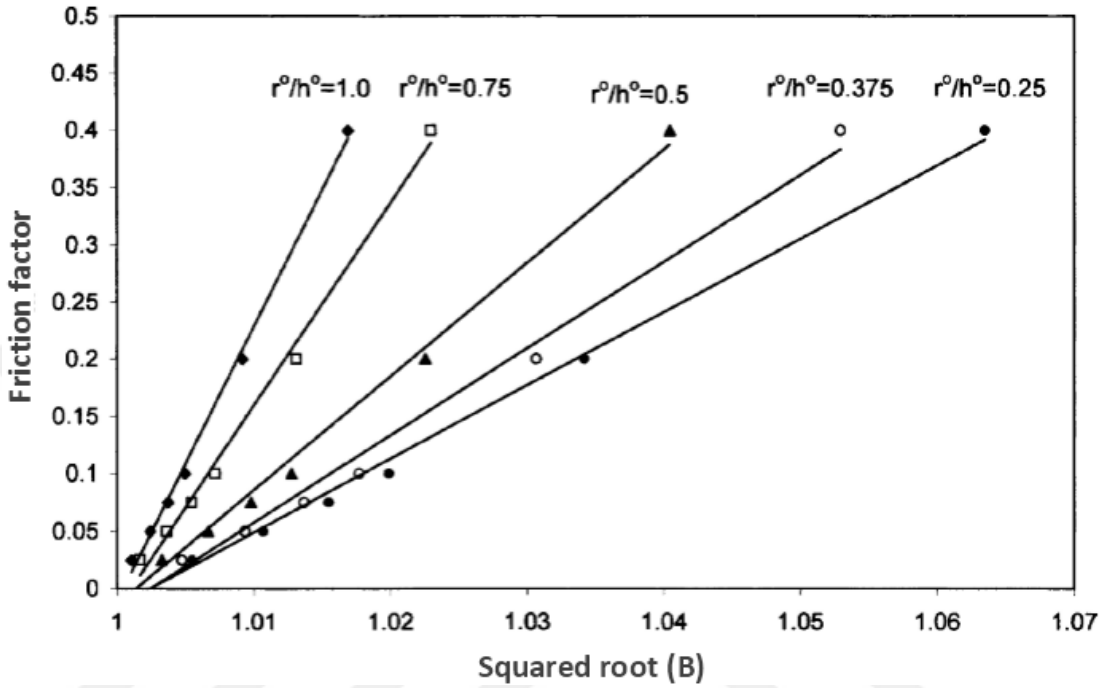

Figure 19- The relationship between Friction factor and squared root B[23]

After determining friction coefficient, excessive stress values can be corrected by using Equation 12 for high friction coefficients:

$$\sigma_a = \sigma_{fc}\left[\left(\frac{1}{\mu}\right)\left(\frac{h}{d}\right)\right]^2 \left[\exp\left(\mu\frac{d}{h}\right) - \left(\mu\frac{d}{h}\right) - 1\right] \tag{12}$$

In the equation, σ_a (uncorrected) is determined from the length extensometer, and σ_{fc} is the stress after the friction correction. d and h denote the time-dependent diameter and height data, μ is the friction coefficient.

For low friction coefficients, equation 12 is reduced to simplified equation by applying a first order Taylor Series Expansion:

$$\sigma_a = \sigma_{fc}[1 + \tfrac{1}{3}\mu(\tfrac{d}{h})] \tag{13}$$

The simplified approach is used for the remaining evaluations since the amount of barreling in the experiments is relatively low.

An example is presented in Figure 20 to illustrate the effect of Evan's and Ebrahimi's correction. As can be seen from the example, the friction causes an increase in the measured stress. Stress increases as the deformation of the part increases. The differences between uncorrected and corrected stress-strain curves vary from 12% to 13% for Ebrahimi's approach and %2 to 13% for Evans's approach at 0.4 strain with different strain rates and temperature. As can be understood from the percentage differences, the effect of temperature and strain rate did not change the friction coefficients when Ebrahimi's approach was applied. It is very difficult to demonstrate the complicated triaxial compression test with simplified and hypothetical analytical calculations. Evans obtained friction coefficients which are influenced by temperature and strain rate using the Finite Element Method and derives the calibration curves for different situations. Therefore, the friction correction required for flow curves was achieved by the approach of Evans.

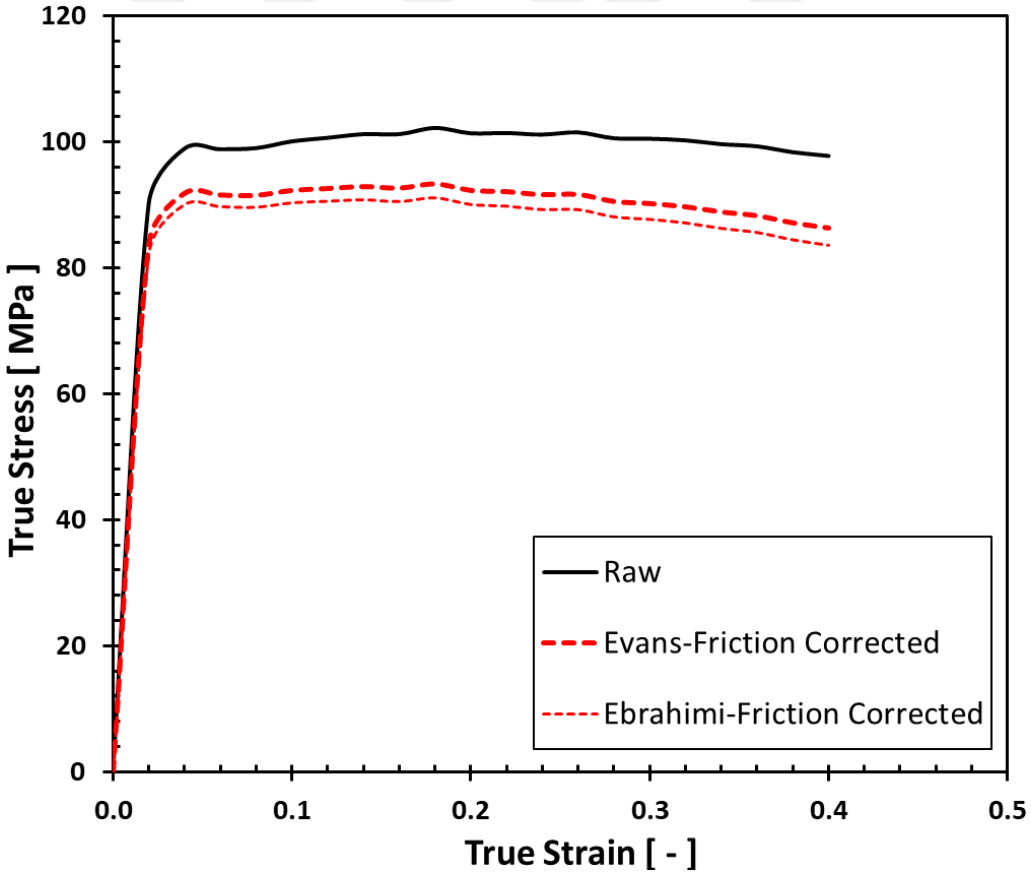

Figure 20- Comparison of friction correction between Evans & Ebrahimi approach

3.1.4 Deformation Heating Correction

While the material is deformed, most of the mechanical work done is released as a heat. The heat generated during the slow-speed tests, where the convectional heating is negligible due to high vacuum atmosphere, is transferred to the jaws by conduction and after to the environment by radiation. Therefore, no temperature increase is observed and the isothermal conditions are maintained. However, since there is not enough time for the heat generated in the high-speed tests to be released, an increase in the specimen temperature is observed throughout the test.

The deformation heat causes an increase in the specimen temperature during the test and causes a miscalculation of the actual flow stress. There are several approaches in the literature for removing deformation heat. Since the Gleeble System has thermocouple data to measure the temperature increase during deformation, the method that takes advantage of this situation is preferred. To compensate deformation heating, Equation 14[25] is applied as follows.

$$\sigma_0 = \sigma_{fc} - \Delta T \frac{\partial \sigma}{\partial T}\Big|_{\varepsilon,\dot{\varepsilon}} \tag{14}$$

In the equation, time dependent σ_o is the uncorrected stress and ΔT is the temperature rise at any time during the test. $\partial\sigma/\partial T$ denotes the change in the stress of the material at a constant strain rate and at a certain strain with respect to temperature. The $\partial\sigma/\partial T$ value is not a directly known value, but it can be estimated by taking advantage of different temperatures and at the same strain rate. The results show that there is a linear relationship between stress and temperature at certain strain values. Since the test matrix is wide, the value of $\partial\sigma/\partial T$ is obtained by using multi-linear regression analysis.

When the test results were examined, it was seen that deformation heating is dominant in relative high-speed ($>0.1 s^{-1}$) and low temperature (900°C<) due to the higher stress occurred in these tests. The temperature rise during 850°C with 10^2 s^{-1} and 1000°C with 10^{-3} s^{-1} test is approximately 30°C and 2°C, respectively. The differences between only friction corrected and friction-deformation corrected stress-strain curves vary from 4.5% to 14% at strain 0.4 with different strain rates and temperature. Figure 21 shows the deformation heating correction after friction correction.

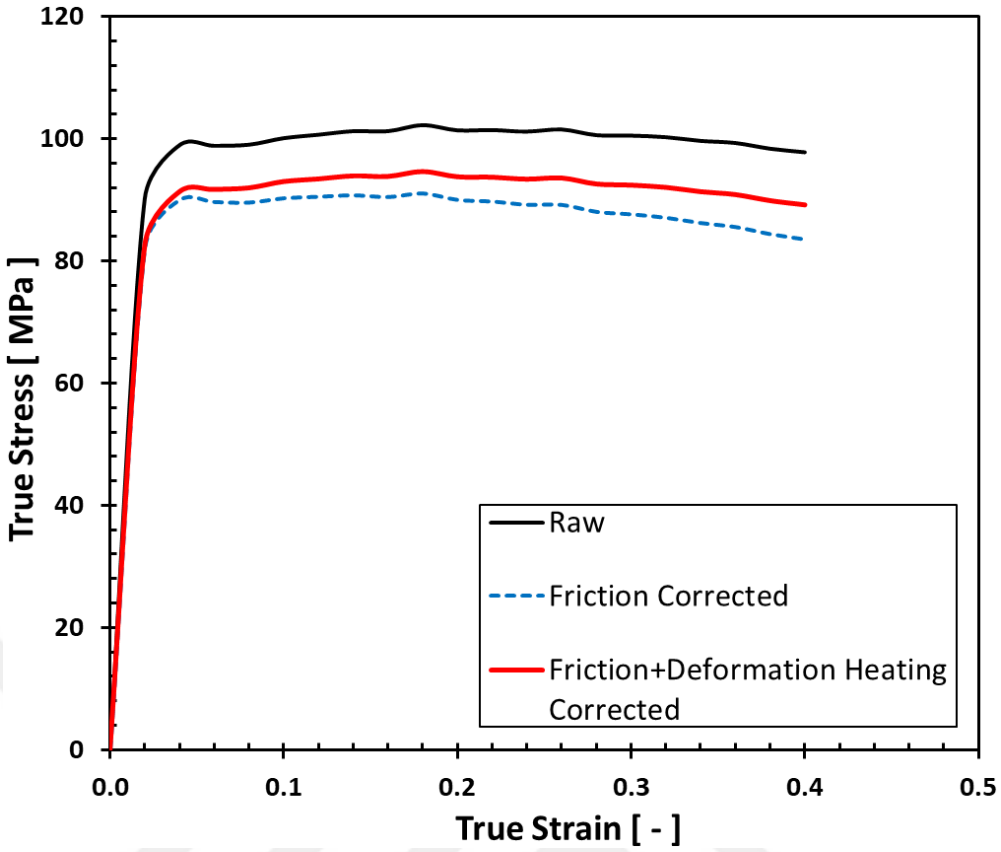

Figure 21- Friction and deformation heating correction of 900°C-10^{-1} strain rate test

3.1.5 Load Cell Ringing Correction

The behavior of materials is sensitive to strain rate. For this reason, making measurements in an appropriate way is very important and physical models require high precision data to get realistic results. Especially in high strain experiments, this is even more difficult.

In high strain test, elements of the test machine are exposed to high forces and this makes the test frame and especially load cell to vibrate strongly. The dynamic effects cause periodic fluctuations in the force data by reaching the natural frequency of the load cell. This leads to incorrect force measurement of the load cell.

In order to remove these effects, it is necessary to perform spectral analysis of the force-time curve and to determine the natural frequency of the device and to filter this frequency from the signal[26]. The commonly used method for spectral analysis is FFT (Fast Fourier Transform) method.

In compression tests, load cell ringing was observed in the 10 s^{-1} and 100 s^{-1} experiments. Since the effect on 10 s^{-1} experiments was quite low, it was eliminated in data reduction and subsequent data processing. However, very high intensity fluctuations were observed in the 100 s^{-1} experiments. For this reason, only these experiments were corrected.

In 850°C and 900°C 100 s^{-1} experiments, load cell ringing is more frequent and severe due to high strength of the material. For this reason, a wider spectrum is filtered out in the FFT analysis. The "FFT Filter" tool of Origin Lab® software was used for spectral analysis and filtering. The process and result made in Figure 22, 23 are exemplified.

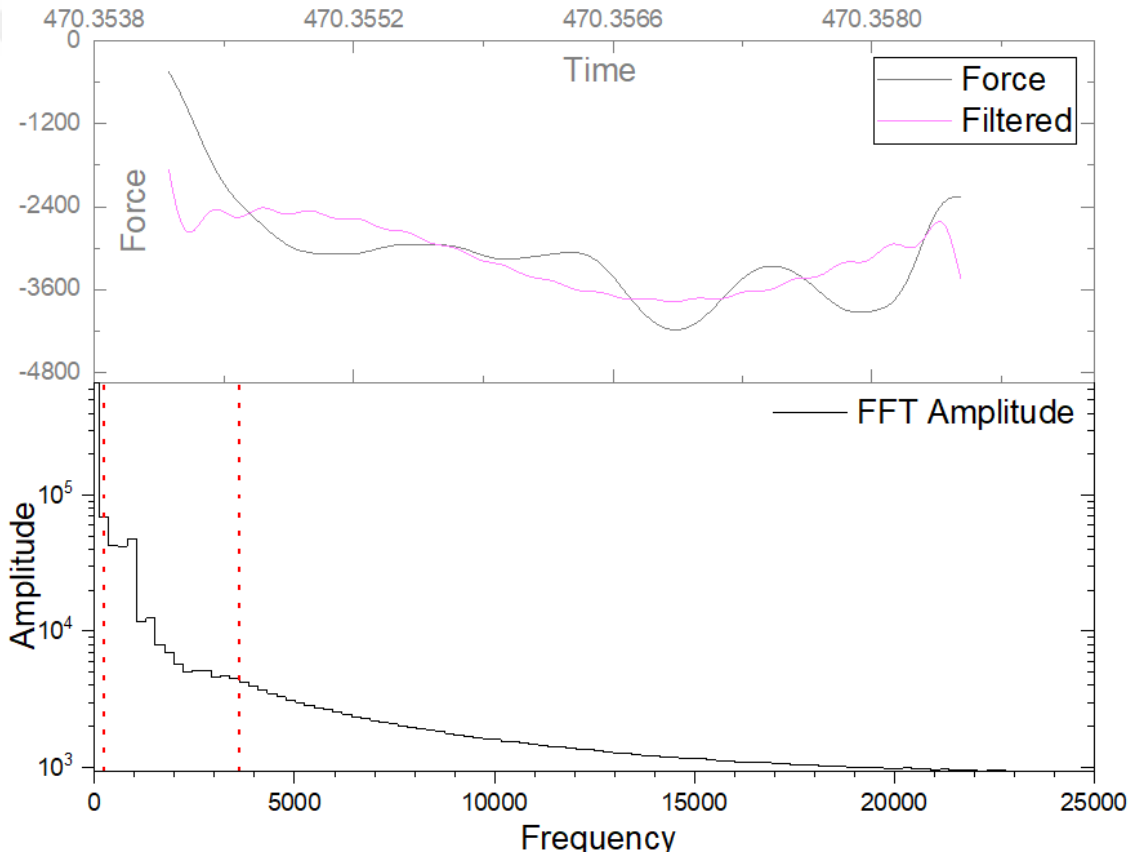

Figure 22- The result of the force data after FFT filter method

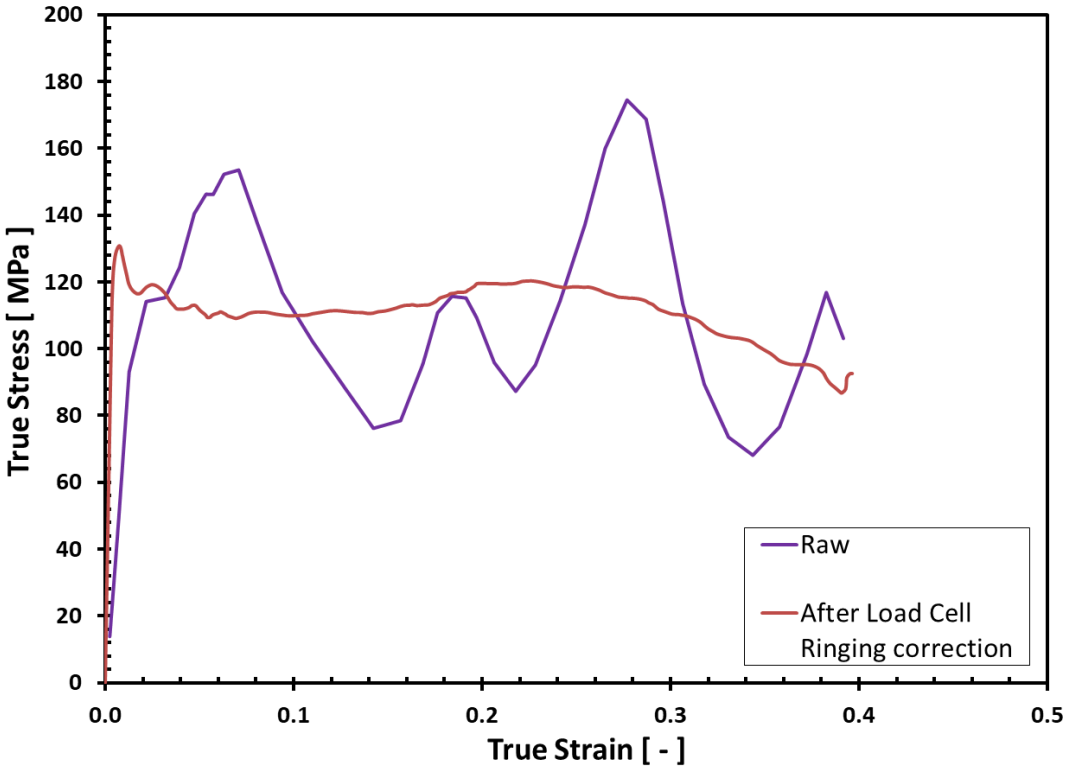

Figure 23- True stress-True strain graph after load cell ringing correction

3.2 Determination of Constitutive Law

The flow curves obtained for the forging process simulation should be expressed in terms of a rheological law. The flow curves obtained from independent experiments are transformed into continuous functions including the process interval by rheological law. The Hänsel-Spittel law, which considers strain, strain rate and temperature, in Equation 15 is widely used in hot forging simulations as it is a universal equation.

$$\sigma_f = Ae^{m_1 T}\varepsilon^{m_2}\dot{\varepsilon}^{m_3}e^{\frac{m_4}{\varepsilon}}(1+\varepsilon)^{m_5 T}e^{m_7\varepsilon}\dot{\varepsilon}^{m_8}T^{m_9} \quad (15)$$

In the equation ε, $\dot{\varepsilon}$ and T respectively indicate strain, strain rate and temperature. *A*, *m1*, *m2*, *m3*, *m4*, *m5*, *m7*, *m8* and *m9* are constants that must be specified. The solution of this 10 non-linear nonlinear system requires non-linear inverse analysis.

The MS excel solver tool was used to determine the Hänsel-Spittel model parameters. Using the "GRG nonlinear method", the normalized root mean square error sum was

reduced as small as possible and fitted to the flow curves which were subjected to certain corrections after being obtained from the experiments.

One of the main difficulties of the analysis is to determine the singular physical solution. As the number of parameters increases, the number of non-physical solutions increases. Five constants (*A, m1, m2, m3, m4*) were sufficient to adequately characterize the yield curves obtained.

In addition to these difficulties, a single set of parameters was not sufficient for all results, as data set was a wide range of temperature and strain rates. Using the obtained results in Hänsel-Spittel calculations, a separate parameter group for strain rates of 0.001, 0.01 and 0.1 and a separate parameter group for strain rates of 1, 10 and 100 were calculated and fitted to the experimental data. The obtained parameters, results and percentage errors in Table 9, 10, 11 and Figure 24, 25 respectively.

850 °C ≤ T ≤ 1000 °C **0.001 s^{-1} ≤ $\dot{\varepsilon}$ ≤ 0.1 s^{-1}** **0.02 ≤ε≤ 0.4**				
A [MPa]	**m_1**	**m_2**	**m_3**	**m_4**
9402706	*-0.01224*	*0.010001*	*0.25149*	*-0.00655*

Table 9- Hänsel-Spittel parameters for low strain rates of Ti-64

850 °C ≤ T ≤ 1000 °C **1 s^{-1} ≤ $\dot{\varepsilon}$ ≤ 100 s^{-1}** **0.02 ≤ε≤ 0.4**				
A [MPa]	**m_1**	**m_2**	**m_3**	**m_4**
604041	*-0.00918*	*0.03211*	*0.14251*	*-0.0051*

Table 10- Hänsel-Spittel parameters for high strain rates of Ti-64

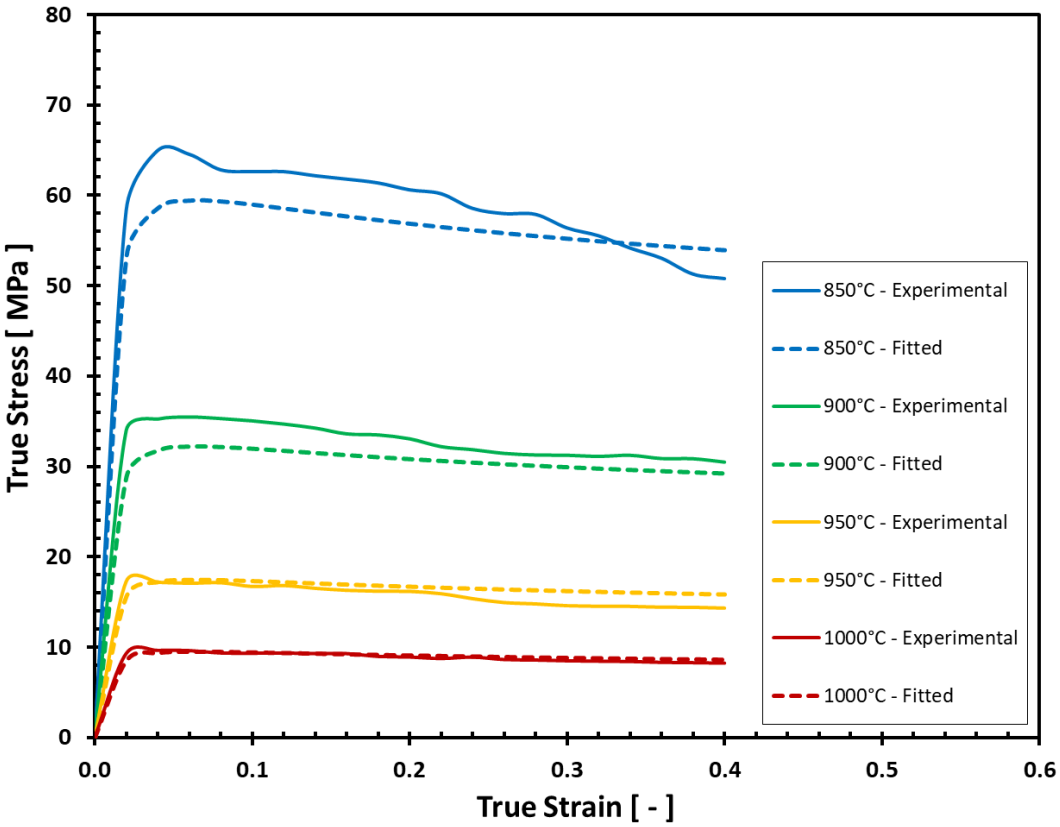

Figure 24- A sample of fitting curves of $0.001s^{-1}$ vs. experimental data

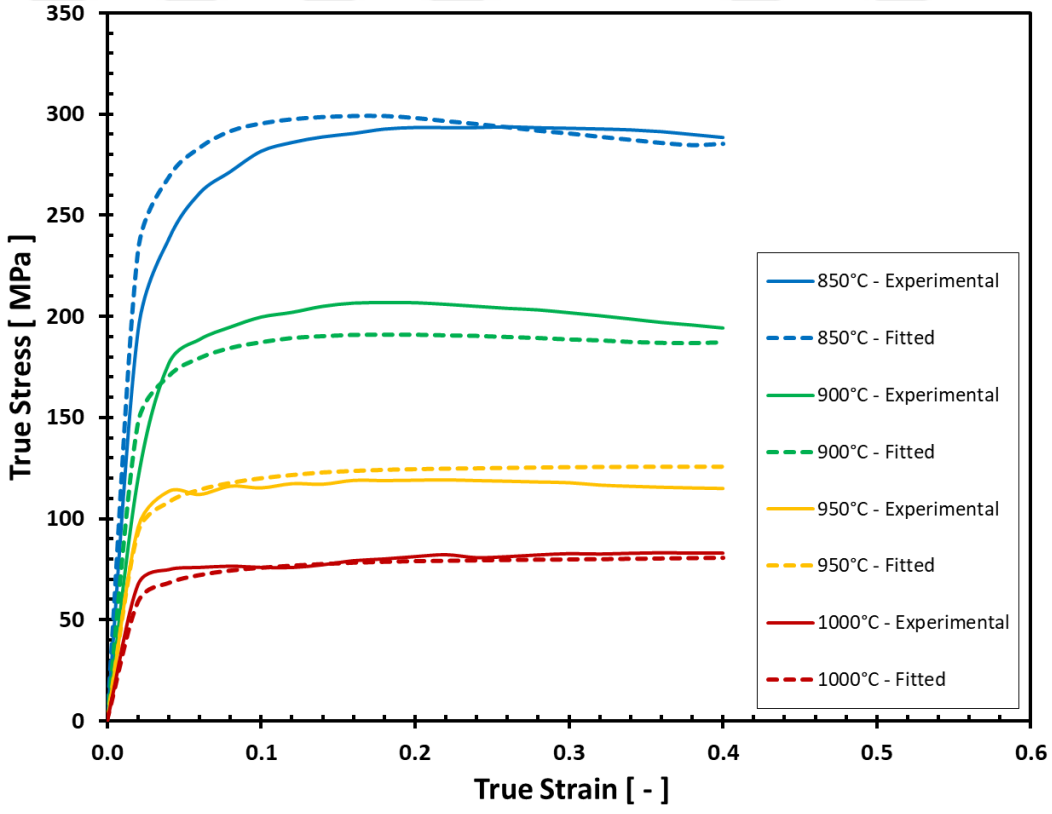

Figure 25- A sample of fitting curves of $10s^{-1}$ vs. experimental data

%	850°C	900°C	950°C	1000°C
0.001 s^{-1}	5.37	6.7	6.49	2.62
0.01 s^{-1}	5.15	3.11	9.94	6.59
0.1 s^{-1}	8.79	4.04	2.41	5.48
1 s^{-1}	10.91	6.06	6.62	10.79
10 s^{-1}	3.97	6.88	5.32	3.24
100 s^{-1}	7.42	6.25	2.42	11.41

Table 11- The average percentage errors between experimental and fitted curves

The validity of the constitutive equation was calculated by the mean absolute error (δ), which is stated as follows:

$$\delta = \frac{1}{N}\sum_{i=1}^{N}\left|\frac{\sigma_{i,exp} - \sigma_{i,cal}}{\sigma_{i,cal}}\right| * 100\% \quad (16)$$

Where N is the reduced data used in the calculation. $\sigma_{i,exp}$ and $\sigma_{i,cal}$ are the values of corrected experimental stress and calculated flow stress, respectively.

The smallest and largest errors occurred at 950°C – 0.1s^{-1} with %2.41 and at 1000°C – 100s^{-1} with %11.41, respectively. As can be seen from the error amounts, there is a good relationship between test results and theoretical calculations, where shows the effective estimation of the applied constitutive equation.

Among the obtained mathematical results, the extrapolation behavior of the function was examined to check if the results present physical solutions. In addition to that temperatures (800°C and 1050°C) which were not included in the test parameters, but which can be considered as hot forming temperature, were also examined by the obtained continuous equation parameters and all the results are presented in Figure 26.

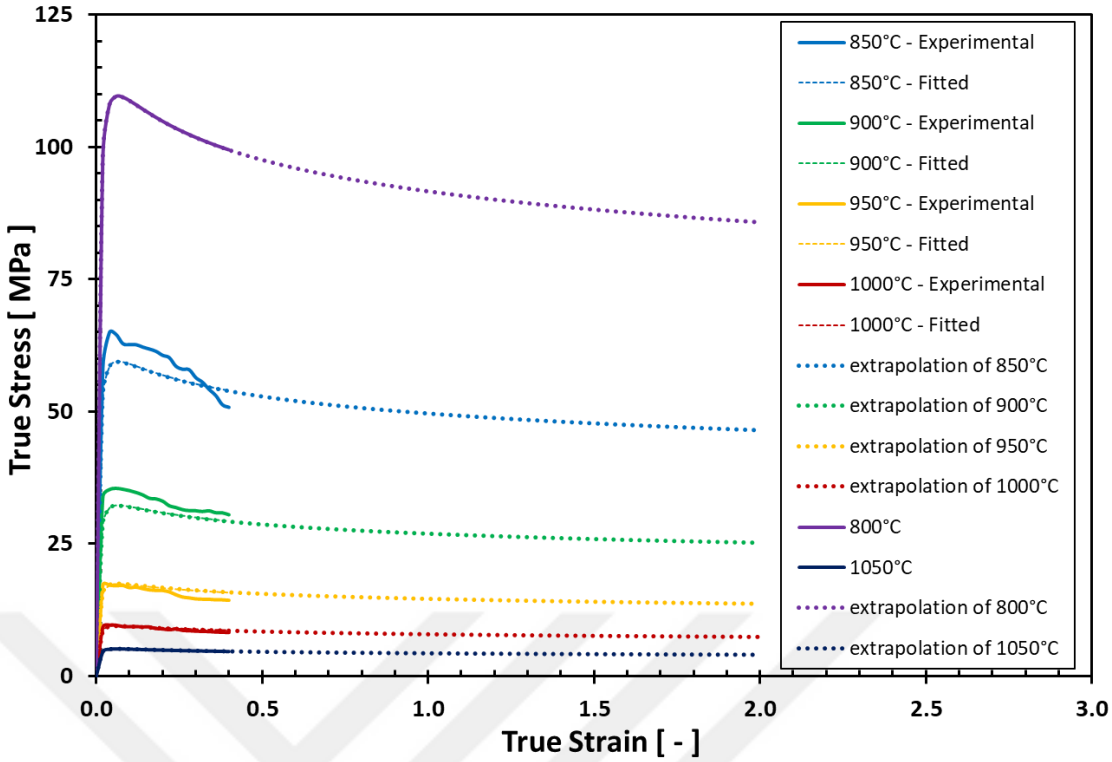

Figure 26- Extrapolation for fitted curves and theoretical calculations of different temperatures at $0.001s^{-1}$

The results show that the extrapolated curves are physical. Besides, Hänsel-Spittel parameters produce reasonable results and extrapolation behavior for near temperatures which were not included when obtaining parameters. However, presented outcomes should be supported and proved by running several FEA.

CHAPTER 4

DETERMINATION OF PROCESS MAP

A processing map is a representation of the behavior of a material, from the point of deformation mechanism, to be imposed process parameters and comprise of a superimposition of efficiency and instability maps[27].

In the design of hot forming processes, while the flow curves are required to determine the material flow and loads, the process map is necessary to determine the temperature and strain rate ranges that must be followed to obtain the product with no defects and desired properties.

The flow behavior of titanium is strongly influenced by process parameters such as strain, strain rate and temperature. In addition, the composition of the material and the initial microstructure affect the flow behavior of these alloys. The content of interstitial elements such as oxygen, nitrogen, carbon and iron also influence the properties of the alloys. For this reason, the process map should be determined by taking into consideration of these important parameters.

Experimental data of flow stress as a function of temperature, strain and strain rate is used to create processing map. It is necessary to conduct a proper and reliable experimental technique for creating them. In Figure 27, determined process maps by Prasad for commercial and ELI (extra low interstitial) grade of Ti64 with equiaxed ($\alpha+\beta$) and β-transformed microstructure are presented. As can be understood from the maps, depending on the initial microstructure, efficiency values and instability regions were shaped and different domains were formed accordingly.

Efficiency and instability maps were created using the “contour map” tool of the “Originlab” program. Maps were plotted on the same scale to plot the final process map.

The contour numbers indicate the efficiency and shaded areas shows unstable regions. It can be seen that several efficiency hills, which come along as domains with consecutively increasing isoefficiency contours, is exposed in the contour map. The

valley that separate domains called as bifurcations. Microstructural mechanism which contributes to the efficiency can be seen in each of the domains[28].

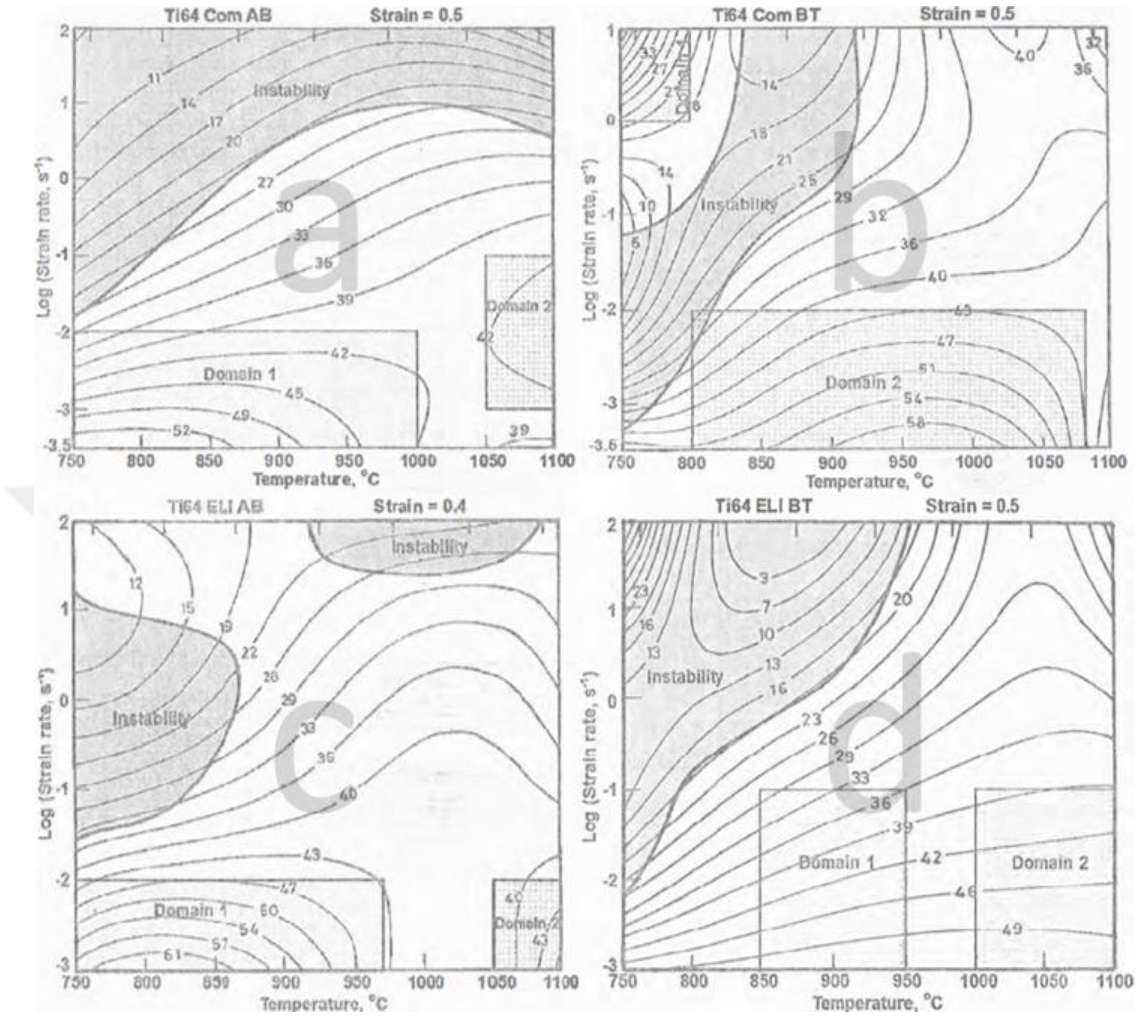

Figure 27- Processing map for different types of Ti64 **a)** Ti64 Commercial α+β **b)** Ti64 Commercial β transformed **c)** Ti64 ELI α+β **d)** Ti64 ELI β transformed[28]

4.1.1 Efficiency Map

The efficiency map is a 3D surface showing the efficiency of the transformation of the work to deformation on the work piece, which is subjected to hot deformation and is a non-linear power dissipater, according to the temperature and strain rate. The final properties after forming depend on the microstructure and cooling conditions. For these reasons, efficiency maps provide information about the final properties of the work piece. Efficiency maps are used to obtain the desired microstructure as well as to estimate the microstructure distribution on the work piece.

The formability is also dependent on the microstructure of the material as well as the state-of-stress, strain rate and temperature in the deformation zone. The stress-strain curves show the reaction of the material to the strain rate and the temperature depending on the hot deformation mechanisms. Different deformation mechanisms can cause similar stress-strain behavior. For this reason, the deformation mechanisms should not be determined only by looking at the shape of the stress-strain curves. There are several deformation mechanisms during hot deformation of the material and some of them are Dynamic Recrystallization (DRX), Superplastic Forming (SPF), Dynamic Recovery (DR), Wedge Cracking (WC), Void Formation (VF) etc. Efficiency values are related to the deformation mechanisms and the microstructure changes that occur parallel to them.

Dynamic recrystallization refers to simultaneous nucleation and growth process during deformation. The DRX reconstitute the microstructure by ensuring the steady flow and good formability. For this reason, DRX is the most preferred process window which optimize hot forming ability and to control the microstructure.

Fine grained materials are able to make extraordinary stretches when deformed at very low speeds and at high temperatures, and this is called superplastic forming. Along with being a safe mechanism, isothermal conditions are needed because of being a slow process.

In dynamic recovery, the density of dislocations is reduced by diffusion. It occurs at lower temperatures than DRX and is therefore a mechanism that occurs more often in warm forming processes. DR causes the material to harden but the hardening speed is lower than the cold forming.

In wedge cracking mechanism, at low strain rates and high temperatures, high stress concentrations occur due to grain boundary sliding, especially at the triple-grain boundary junctions. The formation of the wedge cracking reduce this stress concentration and this is an undesirable mechanism.

Void formation is called as debonding and cracking of the interface in microstructures, where there are hard particles on a soft matrix, due to deformation. This is due to the fact that hard particles do not deform when the main body is under plastic flowing. An undesired mechanism, VF, is effective at low temperatures and high strain rates[28].

In order to obtain the efficiency map, compression tests is needed at different temperature and strain rates. The compression tests used to obtain the flow curves can also be used to determine the efficiency map.

The power dissipation occurs at any moment during the deformation by two complementary processes. The great majority of dissipation occurs with heat during plastic deformation while the rest cause microstructure changes. The strain rate sensitivity of the flow stress determines the power shared between the two processes, and this is an integrity for ideal-linear dissipater. The power absorbed by the work piece during the plastic flow is calculated as follows:

$$\sigma.\dot{\varepsilon} = \int_0^{\dot{\varepsilon}} \sigma.d\dot{\varepsilon} + \int_0^{\sigma} \dot{\varepsilon}.d\sigma \tag{17}$$

or

$$P = G + J \tag{18}$$

The G term represents the power dissipation, most of which is transformed into heat and made by plastic work while the remainder part is stored as a lattice defect. J represents a dynamically formed metallurgical mechanisms. The dynamic material behavior can be modeled explicitly, depending on the variations in the term J. At any temperature or strain, the shared power can be expressed by using the equation 19:

$$\left(\frac{\partial J}{\partial G}\right)\varepsilon, \mathrm{T} = \left(\frac{\partial ln\sigma}{\partial ln\dot{\varepsilon}}\right)\varepsilon, \mathrm{T} \tag{19}$$

which can be defined as the strain rate sensitivity of the material. From equation 19, it also follows that the dynamic constitutive equation is of the type:

$$\sigma = \mathrm{A}\,\dot{\varepsilon}^{\,\mathrm{m}} \tag{20}$$

The value of J at any deformation temperature can be calculated by integrating equation 20:

$$J = \int_0^{\sigma} \dot{\varepsilon}.d\sigma = \frac{\sigma.\dot{\varepsilon}.m}{m+1} \tag{21}$$

Using the equation 21, the J value can be evaluated from the flow stress and the strain rate sensitivity at any given temperature and strain rate. The value of J takes its maximum value when m=1 and the work piece acts as a linear dissipater:

$$J^{max} = \frac{\sigma.\dot{\varepsilon}}{2} \tag{22}$$

The efficiency of power dissipation of work piece is obtained by the ratio of ideal dissipater with power dissipation through microstructure change and calculated as follows[27]:

$$\eta = \frac{J}{J_{max}} = \frac{2m}{m+1} \tag{23}$$

The strain rate sensitivity was determined by the approximation at 0.4 strain as in equation 24:

$$m \cong \frac{\ln(\frac{\sigma_2}{\sigma_1})}{ln\frac{\sigma_2}{\sigma_1}} \tag{24}$$

Where the corresponding flow stresses are the values at each strain rate forward extrapolated to the instant of the change. For the calculation of m value of 100 s^{-1}, trendline was fitted to the log strain rate - strain rate sensitivity parameter graph and the line equation was used to obtain m value for 100 s^{-1} tests. Figure 28 shows an example of relationship between strain rate sensitivity and strain rate.

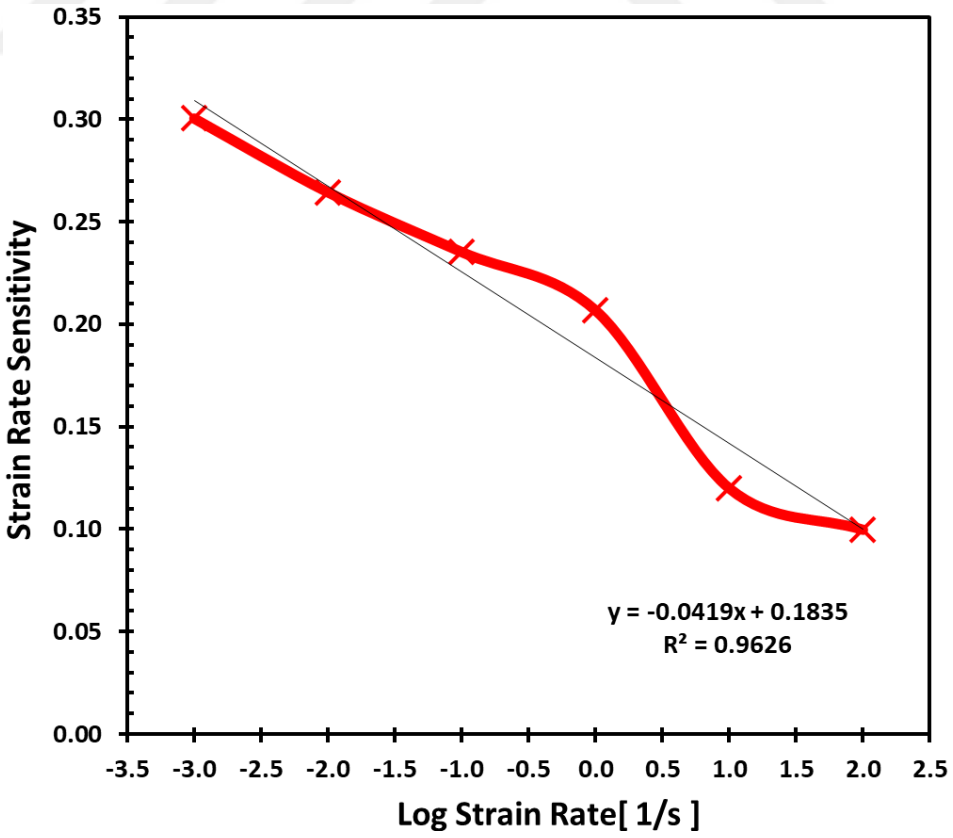

Figure 28- An example of relationship between strain rate sensitivity and strain rate

The variation of η with temperature and strain rate forms the efficiency map that shows the microstructure change and deformation mechanisms.

When the results shown in Figure 29 are examined, the beta transus (~970°C) shows itself by inflecting the efficiency contours. The maximum efficiency appears at 0.001 s^{-1} and deformation temperature 1000°C. This small area may represent the dynamic recrystallization of the β phase. A domain in the range 0.001 – 0.01 s^{-1} and 850 – 975°C have efficiency values above 40 and may correspond to superplastic forming[28]. At strain rate ranges 0.01 – 1 s^{-1} and 925 – 1000°C, the material can be considered exhibiting dynamic recrystallization[28].

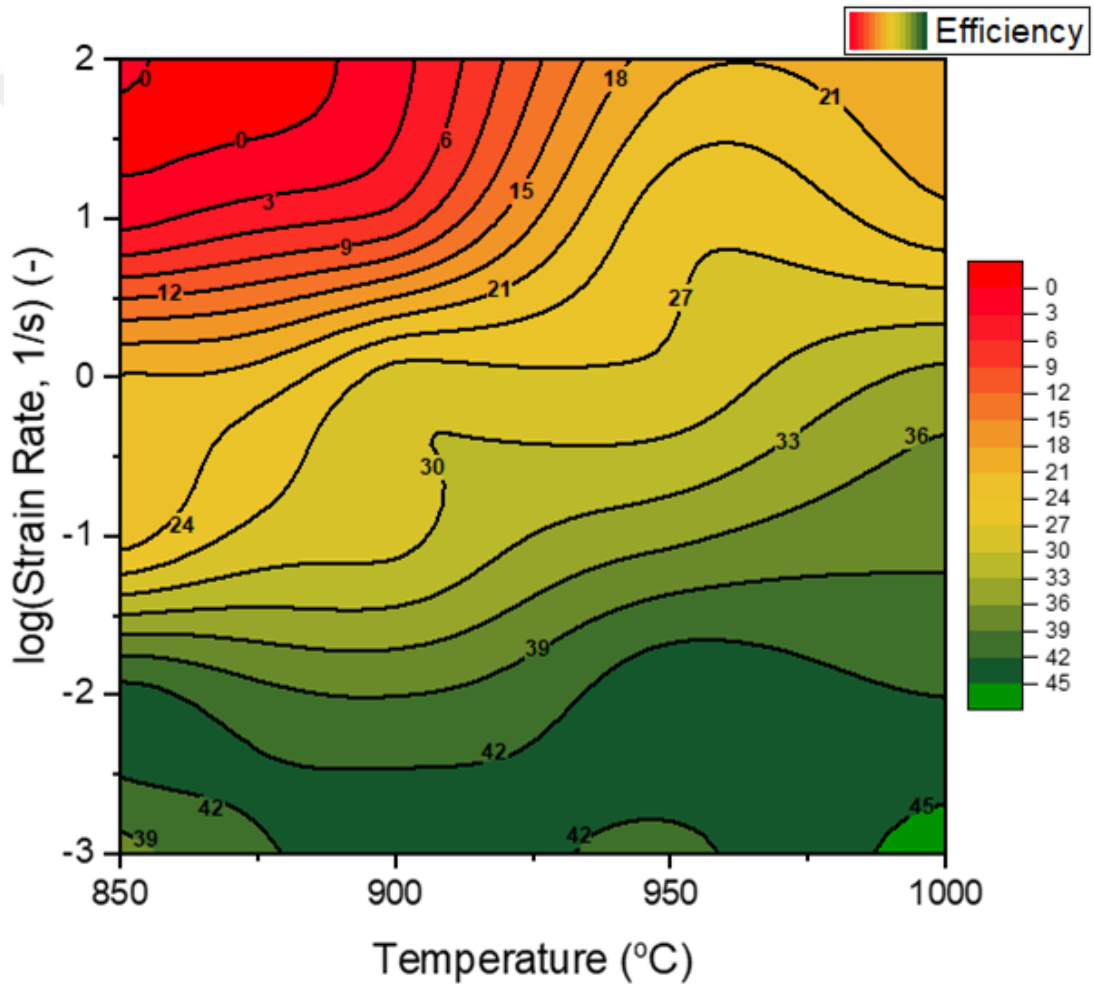

Figure 29- Efficiency map of Ti64 for 850 - 1000°C and 10^{-3} - 10^{2} s^{-1}

4.1.2 Instability Map

Instability maps can be obtained from flow curves similar to efficiency maps. Stabilization condition is defined in Ziegler's dynamic material model study[29]. Stable flow will occur if the differential quotient satisfies the inequality:

$$\frac{dD}{dR} > \frac{D}{R} \tag{25}$$

Where R=$\sqrt{\dot{\varepsilon}.\dot{\varepsilon}}$ and D is the dissipative function that represents the constitutive behavior of the material. J is the dissipation function that shows metallurgical stability because it determines the dissipation through metallurgical process. By putting D = J in Equation 25, one obtains the condition for microstructural stability at in terms of a dimensionless parameter[28]:

$$\xi = \frac{\partial\left(\ln\left(\frac{m}{m+1}\right)\right)}{\partial \ln(\dot{\varepsilon})} + m \tag{26}$$

In this method, the regions where the unsteady flow parameter takes a negative value are the regions with possible unstable flow[5].

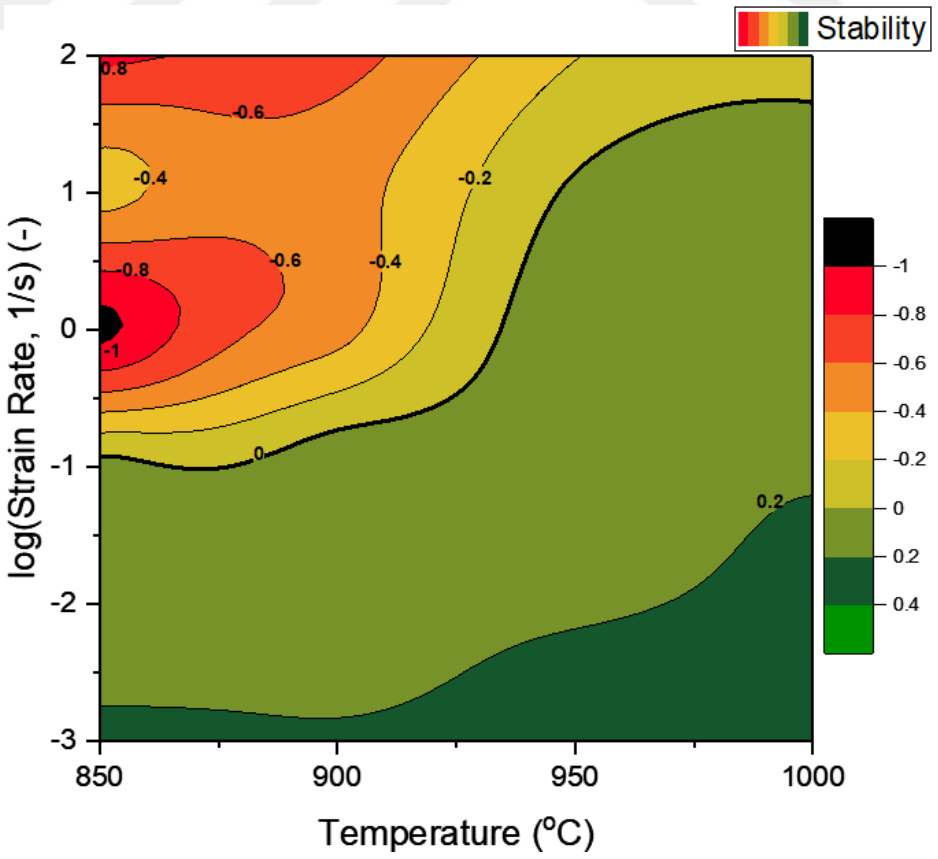

Figure 30- Instability map of Ti64 for 850-1000°C and 10^{-3} - 10^{2} s^{-1}

Figure 30 presents that even relatively high strain rates exhibits flow instabilities. During the plastic forming of Ti-64 in the range strain rates of >0.1 s^{-1} at 850-925°C, flow instability may occur. It can be determined that increasing temperature decrease the instabilities in deformed part for this temperature and strain rate range.

When the efficiency and instability maps superimposed as in Figure 31, it can be seen that formability regions, which obtained from them separately, coincide with together. This shows that there is a good correlation between efficiency and instability methods.

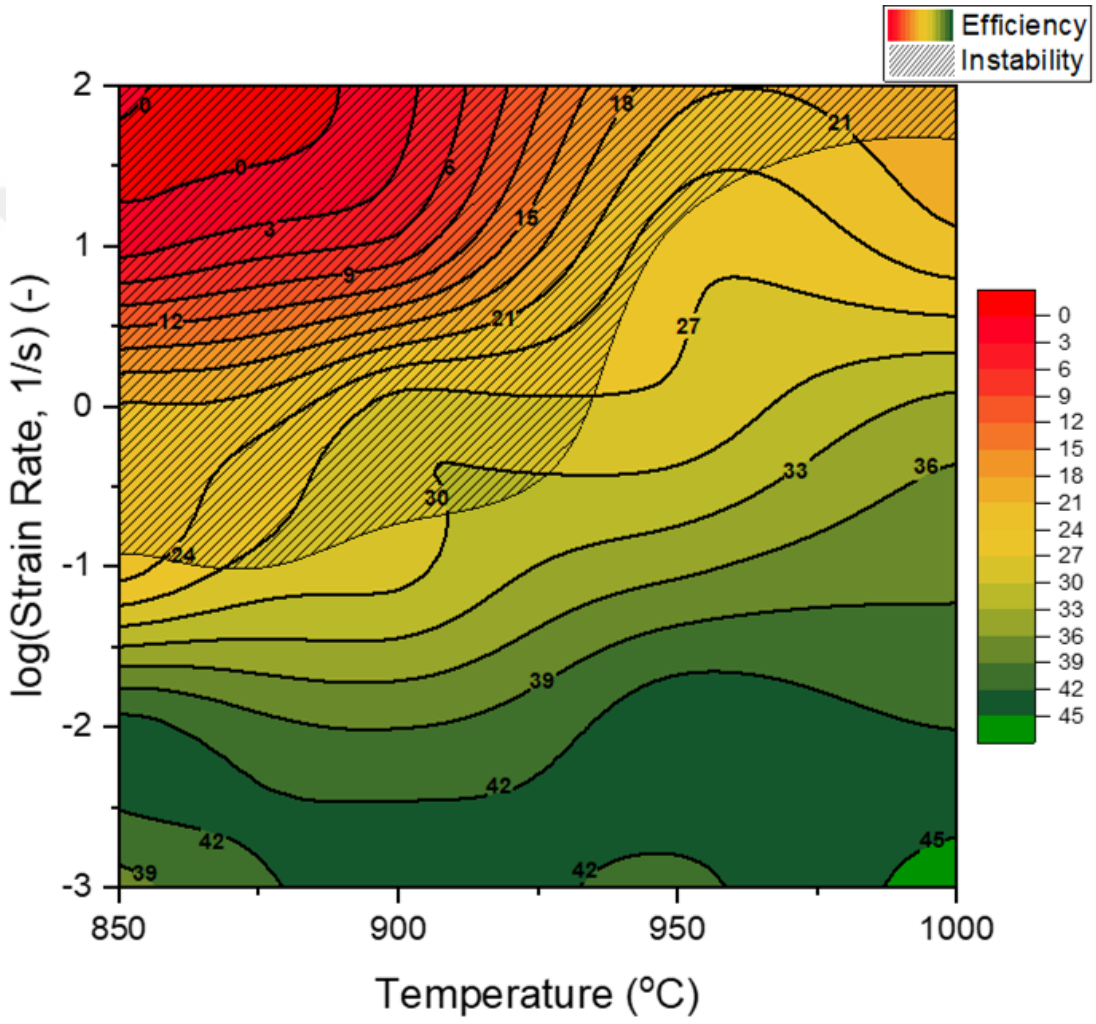

Figure 31- Process map of Ti64 for 850-1000°C and 10^{-3} - 10^{2} s^{-1}

When the process map of Ti64 examined, with an efficiency value of around 30 and above can be considered safe to deform the material , while areas below 30 are unstable relative to instability maps and flow localization can be observed[28]. The map shows that >0.1 s^{-1} strain rate is not suitable for hot forming in the range of 850-925°C while

100 s^{-1} is not suitable at any temperature. A manifestation were created in Table 12 to show processing conditions for Ti64 according to the obtained process map.

Manifestation	**Temperature, °C**	**Strain Rate, s^{-1}**
Superplasticity of α+β	850 – 975	0.001 – 0.01
DRX of β	975 – 1000	0.001
Flow Instability	850 – 925 950 – 1000	>0.1 >10

Table 12- Processing conditions for Ti-64

When the obtained process map were compared with Prasad's α+β Ti64 process map, even the maps look similar, there are important differences in terms of efficiency values and instability regions and also at bifurcations and valley formations. For this reason the process map should be determined for a specific material to be used in a real process.

Suitable areas for forming the Ti64 on the process map can present important markers for the types of presses and forming methods that can be used.

Isothermal forging, namely superplastic forming, can be carried out with a low-speed hydraulic press in the range of 0.001 – 0.01 s^{-1} and 850 – 975°C.

Conventional rolling processes start with high temperature and low strain rate and end with low temperature and high strain rates. On the obtained map, rolling can be performed in a very narrow region, from 1 – 10 s^{-1} and 950 – 1000°C. Also, since the beta transus point on this region, this may cause texture changes in Ti64, which has a two-phase structure, and detailed microstructure and texture analysis is required.

Hammer forging with high strain rate principle will most likely cause undesired mechanical and microstructural properties according to the obtained process map.

As a result, the obtained domains for α+β Ti64 offer a narrow formability region. Therefore, α+β or β-transformed ELI grade or β-transformed commercial, which offer a wide range of formability domain and are more suitable for forging industrial conditions, should be used.

CONCLUSIONS AND FUTURE WORK

Titanium alloys are commonly used in the field of aviation because of their resistance to corrosion as well as their lightness and strength. The problems such as flow instabilities, macro-micro cracks and heterogeneous microstructure during hot deformation need to be solved by designing a thermo-mechanical process.

This study aims to develop a processing map which presents the instability and formability regions in order to visualize a general deformation behavior. For this reason, several compression tests in a wide range of temperature and strain rate carried out for the aim of this study. Obtained true stress - true strain curves were put a series of process to determine the flow curves. Flow curves were used to create efficiency and instability maps. The deformation behavior evaluated by the Dynamic Material Model.

Generated process map shows that increasing strain rate and decreasing temperature can lead to flow instabilities. The peak efficiency obtained at strain rate of 10^{-3} s^{-1} and deformation temperature 1000°C which means that the condition correspond to the optimum condition for thermo-mechanical processing. In terms of forging with mechanical presses, the range of 950-1000°C may be considered to perform forging process. Unstable regions are observed in the range of strain rates $>10^{-1}$ s^{-1} at 850-925°C and strain rates $>10^{-1}$ at 950-1000°C.

Future works can be listed as below:

- In order to use the Hänsel-Spittel parameters free of problems in the simulation software, a single parameter can be obtained by performing detailed non-linear regression analysis of the parameters at low and high strain rates.
- It is possible to find out which method is more effective for different temperature and strain rates by calculating the generally accepted Zener-Hollomon parameter and comparing the curves obtained with the Hänsel-Spittel constitutive equation.
- Due to the wide range of test conditions, hypothetical calculations of temperature and strain rate transients cause errors, and the process map only

provides a general idea. With microstructure analysis, the working ranges can be reduced or new process conditions can be added to the intervals to obtain more precise process maps.

- In order to prove the validity of the obtained model parameters, the results should be compared by performing simulations with the finite element analysis method.
- Estimates can be made about the microstructure with the data obtained from the efficiency and instability maps, but microstructure analysis and macro & micro damage analysis methods must be utilized in order to obtain realistic results.

REFERENCES

[1] S. L. Semiatin, V. Seetharaman, and I. Weiss, “The thermomechanical processing of alpha/beta titanium alloys,” *JOM*, vol. 49, no. 6, pp. 33–39, 1997.

[2] Y. V. R. K. Prasad, T. Seshacharyulu, S. C. Medeiros, and W. G. Frazier, “Effect of preform microstructure on the hot working mechanisms in ELI grade Ti–6Al–4V: transformed β *v* . equiaxed ($\alpha + \beta$),” *Mater. Sci. Technol.*, vol. 16, no. 5, pp. 511–516, 2000.

[3] M. F. Ashby and H. J. Frost, “Deformation-mechanism maps,” *Oxford Pergamon Press.*, pp. 44–45, 1982.

[4] R. Raj, “Development of a Processing Map for Use in Warm-Forming and Hot-Forming Processes,” *Metall. Trans. A*, vol. 12, no. 6, pp. 1089–1097, 1981.

[5] S. L. Semiatin and J. J. Jonas, “Formability and workability of metals: plastic instability and flow localization,” *Am. Soc. Met. 1984*, p. 299, 1984.

[6] Y. V. R. K. Prasad *et al.*, “Modeling of dynamic material behavior in hot deformation: Forging of Ti-6242,” *Metall. Trans. A*, vol. 15, no. 10, pp. 1883–1892, 1984.

[7] Y. V. R. K. Prasad, T. Seshacharyulu, S. C. Medeiros, and W. G. Frazier, “Influence of oxygen content on the forging response of equiaxed (α+β) preform of Ti-6Al-4V: Commercial vs. ELI grade,” *J. Mater. Process. Technol.*, vol. 108, no. 3, pp. 320–327, 2001.

[8] A. Łukaszek-Sołek and J. Krawczyk, “Processing Maps of the Ti-6Al-4V Alloy in a Forging Process Design,” *Key Eng. Mater.*, vol. 641, pp. 190–197, 2015.

[9] H. C. Braga, R. Barbosa, and J. Breme, “Hot strength of Ti and Ti6A14V deformed in axial compression,” *Scr. Metall. Mater.*, vol. 28, no. 8, pp. 979–983, 1993.

[10] K. E. Tello, A. P. Gerlich, and P. F. Mendez, “Constants for hot deformation constitutive models for recent experimental data,” *Sci. Technol. Weld. Join.*, vol. 15, no. 3, pp. 260–266, 2010.

[11] N. K. Park, J. T. Yeom, and Y. S. Na, “Characterization of deformation stability in hot forging of conventional Ti-6Al-4V using processing maps,” in *Journal of Materials Processing Technology*, 2002, vol. 130–131, pp. 540–545.

[12] W.-S. Lee and C.-F. Lin, “High-temperature deformation behaviour of Ti6Al4V alloy evaluated by high strain-rate compression tests,” *J. Mater. Process. Technol.*, vol. 75, no. 1–3, pp. 127–136, 1998.

[13] E. Calvert, J. Pollard, M. Jackson, B. Wynne, and R. Thackray, *Determining a flow stress model for high temperature deformation of Ti-6Al-4V*, vol. 828–829. 2015.

[14] P. Opěla *et al.*, “Hot Flow Stress Models of the Steel C45,” *Metalurgija*, vol. 54, no. 3, pp. 469–472, 2015.

[15] S. Suresh, “Acta Materialia: Preface,” *Acta Materialia*, vol. 51, no. 19, p. 5647, 2003.

[16] G. Lütjering, “Influence of processing on microstructure and mechanical properties of (α+β) titanium alloys,” *Mater. Sci. Eng. A*, vol. 243, no. 1–2, pp. 32–45, 1998.

[17] B. Ralph, “Titanium alloys: An atlas of structures and fracture features,” *Mater. Charact.*, vol. 59, no. 3, p. 348, 2008.

[18] T. Choda, H. Oyama, and S. Murakami, “Process designing technologies for titanium alloy forging for aircraft parts,” *R D Res. Dev. Kobe Steel Eng. Reports*, vol. 64, no. 2, pp. 28–32, 2014.

[19] G. E. Dieter and D. Bacon, *Mechanical metallurgy SI Metric Edition*, vol. 273, no. 4. 1988.

[20] G. Systems, “Gleeble Users Training 2013 ®,” *Gleeble users Train.*, 2013.

[21] ASTM, *ASTM E209-00 (2010): Standard Practice for Compression Tests of*

Metallic Materials at Elevated Temperatures with Conventional or Rapid Heating Rates and Strain Rates. 2010.

[22] B. Roebuck, J. D. Lord, and M. Brooks, “Measurement Good Practice Guide No 3 Measuring Flow Stress in Hot Axisymmetric Compression Tests Revised – Summer 2002 * NPL Materials Centre , National Physical Laboratory IRC for Computer Aided Engineering , University of Wales , Swansea,” no. 3, 2002.

[23] R. Ebrahimi and A. Najafizadeh, “A new method for evaluation of friction in bulk metal forming,” *J. Mater. Process. Technol.*, vol. 152, no. 2, pp. 136–143, 2004.

[24] R. W. Evans and P. J. Scharning, “Axisymmetric compression test and hot working properties of alloys,” *Mater. Sci. Technol.*, vol. 17, no. 8, pp. 995–1004, 2001.

[25] D. Zhao, “Temperature correction in compression tests,” *J. Mater. Process. Tech.*, vol. 36, no. 4, pp. 467–471, 1993.

[26] B. Roebuck, M. Brooks, and M. G. Gee, “Load Cell Ringing in High Rate Compression Tests,” *Appl. Mech. Mater.*, vol. 1–2, pp. 205–210, 2004.

[27] Y. V. R. K. Prasad, “Processing maps: A status report,” *J. Mater. Eng. Perform.*, vol. 22, no. 10, pp. 2867–2874, 2013.

[28] Y. V. R. K. Prasad, K. P. Rao, and S. Sasidhara, *Hot working guide: A compendium of processing maps*. 2015.

[29] H. Ziegler, “No Title,” in *Progress in solid mechanics*, vol. Vol.4, 1963, p. 93.

APPENDIX

Compression Test Specimen Drawing